Interaction Notes

~~Sensor and Simulation Notes~~

Note ~~128~~ 75

May 1971

Charge Distribution on a Two-Dimensional Airfoil

by

F. M. Tesche
Northrop Corporate Laboratories
Pasadena, California

Abstract

A conformal mapping technique for determining the charge density on a two-dimensional airfoil having a net charge on it or being immersed in an electro-static field is presented. The charge density on a wide variety of airfoils is plotted as a function of position on the airfoil surface for the case of the airfoils being charged. It is shown how this charge density may be simply related to that arising due to the incident electric field. In addition, curves summarizing the behavior of the charge densities at the leading and trailing edges of the airfoil are given for various airfoil shapes.

The results of this analysis may be utilized in attempting to predict the charge distribution on the wings of an aircraft subject to an electromagnetic pulse (EMP). Moreover, if an aircraft is to be modeled by a thin-wire structure, so as to permit the determination of the low-frequency behavior of the surface currents, the choice of the radius in the wire model for the wings is indicated.

Acknowledgement

The author would like to thank Capt. Carl E. Baum for his many valuable suggestions regarding this work, and Mrs. G. Peralta for her assistance in preparing the manuscript and the curves.

I. Introduction

In attempting to study the behavior of charges and currents induced on an aircraft which is subject to an EMP, the static charge distribution on the aircraft provides a reasonable description of these quantities for the lower portion of the frequency spectrum of the pulse. The determination of the static charge distribution on an actual aircraft is an extremely difficult, if not impossible, task. It is possible however, to consider isolated parts of the aircraft, such as a wing, to obtain an approximate solution to the static problem.

Through the use of conformal mapping techniques, the static charge distribution on a two-dimensional airfoil which is either immersed in an incident electrostatic field, or has a total known charge placed on it, can be computed. This solution can then be used as an approximation to the quasi-static charge distribution on the wings of the aircraft.

If the aircraft is modeled by a thin-wire structure and the time varying values of the total longitudinal current and charge on the aircraft are obtained through a solution of the appropriate integral equation, the results to be presented in this note will indicate how the total charge distributes itself over the airfoil surface. Moreover, this analysis will relate the physical dimensions of the airfoil to the radius of the cylindrical wire that constitutes the wing portions of the thin-wire model of the aircraft.

For cases where the incident time varying electric field is everywhere perpendicular to the thin-wire model of the aircraft, there is no current calculated for the structure. In this case the total charge on the airfoil is zero, but an induced surface charge still exists due to the presence of the incident electric field. This induced charge distribution, as calculated from the conformal mapping technique, will give a more accurate approximation to the actual charge induced on the wings of the aircraft subject to an EMP having this polarization.

II. The Joukowski Transformation

In complex potential theory, a transformation of the form

$$z = w + \ell^2/w \tag{1}$$

is capable of transforming a circle in the complex w plane into an airfoil in the complex z plane. This transformation, known as the Joukowski Transformation[1,2,3], has wide applicability in the field of hydrodynamics.

In studying this transformation, it is possible to verify the following properties:

1. Points in the w plane exterior to the circle $|w| = \ell$ map into the complete z plane.
2. Points in the w plane interior to the circle $|w| = \ell$ also map into the complete z plane, but onto a different Riemann surface than in the first case.
3. Points on the circle $|w| = \ell$ map into the line $-2\ell < z < 2\ell$ in the z plane.
4. A circle in the w plane with radius "a" and center at $w_o e^{j\alpha}$ maps into an airfoil shaped contour in the z plane. This circle is constrained to be outside the region $|w| = \ell$.
5. There are two singular points where $dz/dw = 0$ and the transformation ceases to be conformal. These are at $w = \pm\ell$. The circle of radius "a" which maps into the airfoil can intersect one or both of these singular points, or the singular points can be completely inside of this circle. For those cases where the singular points are enclosed by the circle, the airfoil curve in the z plane has no discontinuities in it, even at the trailing edge.

With this transformation, it is possible to map the circle in the w plane as shown in Fig. 1a into an airfoil in the z plane. For points on the circle of radius "a" denoted by C_a and having a center at $w_c = w_o e^{j\alpha}$, the relation for the airfoil is given by Eq. (1) as

$$z = (w_o e^{j\alpha} + a e^{j\theta}) + \frac{\ell^2}{(w_o e^{j\alpha} + a e^{j\theta})} \tag{2}$$

where θ is the angle shown in Fig. 1a.

In plotting the different possible shapes of airfoils, it is convenient to normalize all lengths by the factor "a". Hence, the above relation can be rewritten as

$$\frac{z}{a} = (e^{j\alpha} w_o/a + e^{j\theta}) + \frac{(\ell/a)^2}{(e^{j\alpha} w_o/a + e^{j\theta})} . \tag{3}$$

In a problem involving an actual airfoil, the value of the parameter "a" is related to the physical size of the airfoil and w_o, ℓ, and α give the shape of the airfoil. More will be said about the values of these parameters in later sections of this note.

III. Airfoil Immersed in a Uniform Electrostatic Field

Consider an incident electric field in the w plane making an angle θ_{inc} with the u axis as shown in Fig. 2b. This incident field can be determined from the complex potential

$$\psi(w) = - E_o w e^{-j\theta_{inc}} \tag{4}$$

through a suitable operation on the real part of ψ. If a conducting circle, C_a, with its center at w = 0 and radius a is introduced in the w plane, it is required that $\mathrm{Re}[\psi(w)] = 0$ for w on this circle so as to provide the proper boundary condition for the electric field on C_a. The expression for the complex potential then becomes

$$\psi(w) = - E_o w e^{-j\theta_{inc}} + E_o \frac{a^2}{w} e^{j\theta_{inc}}. \tag{5}$$

In a similar fashion, the expression for the complex potential for the case of the circle C_a having a center at the point w_c instead of the origin is given by

$$\psi(w) = - E_o (w - w_c) e^{-j\theta_{inc}} + \frac{E_o a^2 e^{j\theta_{inc}}}{(w - w_c)} . \tag{6}$$

As may be easily verified, this potential function has a vanishing real part on the circle C_a where $w = w_c + ae^{j\theta}$, has the correct behavior as w approaches ∞ and is analytic in the region exterior to the circle C_a. Thus, it is the correct potential for evaluating the electric field everywhere exterior to the conducting circular obstacle.

This potential can be transformed to the z plane to enable the calculation of the fields exterior to the conducting airfoil. This is done by simply expressing w as a function of z. From Eq. (1) it is found that

$$w = \frac{1}{2} (z \pm \sqrt{z^2 - 4\ell^2}) \tag{7}$$

where the + sign is to be chosen, since it is desired to consider the mapping

of the region exterior to $|w| = \ell$ into the complete z plane. With this relation, the potential in the z plane which contains the airfoil is expressed as

$$\Phi(z) = - E_o \left[e^{-j\theta_{inc}} \left(\frac{1}{2}(z + \sqrt{z^2 - 4\ell^2}) - w_c \right) + \frac{a^2 e^{j\theta_{inc}}}{\left(\frac{1}{2}(z+\sqrt{z^2-4\ell^2}) - w_c \right)} \right] \qquad (8)$$

Notice that as z approaches ∞ this potential function behaves as $- E_o z e^{-j\theta_{inc}}$ which is the required form for the incident electric field. From $\Phi(z)$ the electric field in the z plane can be found. Letting $\Phi(z) = \phi(x,y) + j\beta(x,y)$, the derivative of Φ with respect to z can be written as

$$\frac{d\Phi}{dz} = \frac{\partial \phi}{\partial x} + j \frac{\partial \beta}{\partial x} = \frac{\partial \phi}{\partial y} - j \frac{\partial \beta}{\partial y} \qquad (9)$$

since Φ is an analytic function of z. Upon noting that $E_x = - \partial\phi/\partial x$ and $E_y = - \partial\phi/\partial y$, Eq. (9) yields the following relation

$$\frac{d\Phi}{dz} = - E_x + jE_y. \qquad (10)$$

On the surface of the airfoil E_x and E_y are such that the total E is perpendicular to the surface since $E_{tan} = 0$. In this case, the charge density σ on the airfoil is given by $\sigma = \varepsilon_o E_\perp$. From Eq. (10), it is then possible to calculate the magnitude of this surface charge density as

$$|\sigma| = \varepsilon_o \left| \frac{d\Phi}{dz} \right|_{z=\text{surface of airfoil}} \qquad (11)$$

In practice it is tedious to use Eq. (11) directly to evaluate $|\sigma|$ due to the complicated dependence on the parameter z. Instead, it is advantageous to rewrite Eq. (11) as

$$|\sigma| = \varepsilon_o \left| \frac{\partial \psi(w)}{\partial w} \frac{\partial w}{\partial z} \right|_{w \text{ on } C_a} . \qquad (12)$$

This form is easier to evaluate.

Taking the derivative of Eq. (6), it is seen that

$$\frac{\partial \psi}{\partial w} = - E_o\left(e^{-j\theta_{inc}} + \frac{a^2 e^{j\theta_{inc}}}{(w-w_c)^2}\right), \tag{13}$$

and similarly, Eq. (1) gives

$$\frac{dw}{dz} = \frac{w^2}{w^2-\ell^2} . \tag{14}$$

The locus of points constrained to lie on the circle C_a, as shown in Fig. 1a, is given by

$$w = w_c + ae^{j\theta} \tag{15}$$

where $w_c = w_o e^{j\alpha}$. Combining Eqs. (13), (14) and (15) gives the required result that

$$|\sigma| = \varepsilon_o E_o \left| \left(e^{-j\theta_{inc}} + e^{j(\theta_{inc}-2\theta)}\right)\left(\frac{1}{1-\ell^2/(w_o e^{j\alpha}+ae^{j\theta})^2}\right)\right| . \tag{16}$$

Upon rearranging and simplifying terms, this last relation can be written as

$$\frac{|\sigma_1|}{\varepsilon_o E_o} = 2\left|\cos(\theta_{inc} - \theta)\right| \left|\frac{1}{1-(\ell/a)^2/(e^{j\alpha}w_o/a+e^{j\theta})^2}\right| . \tag{17}$$

This expression gives the induced surface charge density on the airfoil in the z plane, evaluated at the various points defined by the parameter θ on the circle C_a in the w plane. The subscript 1 on σ indicates that this charge density arises from the incident electric field.

IV. Airfoil with a Net Charge

If the airfoil is no longer immersed in a uniform static field, but has a total charge per unit length Q on it, then the circle in w plane has the same total charge per unit length on it. In the w plane it is possible to write immediately that the complex potential for the charged circle C_a having an origin at w = 0 is given by

$$\psi(w) = \frac{Q}{2\pi\varepsilon_o \ln(w/a)} . \tag{18}$$

If the circle has its center at $w = w_c$, then it is necessary to replace w in Eq. (18) by $w - w_c$.

Using Eq. (12) for the charge distribution on the airfoil, the surface charge is then given by

$$|\sigma_2| = \left| \frac{Q}{2\pi a e^{j\theta}} \left(\frac{1}{1-(\ell/w_o e^{j\alpha}+a e^{j\theta})^2} \right) \right| . \tag{19}$$

Upon simplifying, this last relation becomes

$$\frac{2\pi a|\sigma_2|}{Q} = \left| \frac{1}{1-(\ell/a)^2/(e^{j\alpha}+w_o/a+e^{j\theta})^2} \right| . \tag{20}$$

As in the case of Eq. (17), this gives the normalized surface charge density on the airfoil as a function of the parameter θ. The subscript 2 on σ indicates that this charge density is due to the net charge Q.

It is interesting to note that Eq. (17) for the charge density on the airfoil immersed in an electric field contains the same term as Eq. (20), which gives the charge density in the charged airfoil problem. Moreover, the dependence on the angle of incidence of the electric field is given by a simple multiplicative term, $2|\cos(\theta_{inc} - \theta)|$. As a result, it is necessary to only consider the charged airfoil problem. The charge distribution for the electric field case, expressed as a function of the parameter θ, is then given by:

$$\frac{|\sigma_1|}{\varepsilon_o E_o} = 2|\cos(\theta_{inc} - \theta)| \left(\frac{2\pi a|\sigma_2|}{Q} \right) . \tag{21}$$

Knowing the behavior of the charge density in the case of a charged airfoil, therefore, permits the determination of the charge density on the same airfoil immersed in the uniform electric field.

As mentioned earlier, a thin-wire model of the airfoil yields no induced current or charges on the structure if the electric field is everywhere perependicular to the wires. In such a case, the results for the charge σ_1 arising from a static electric field normal to the Joukowski airfoil would be useful in predicting the behavior of the actual airfoil. For other angles of incidence, the quasi-static electric field incident upon the thin-wire model might be parallel to the wires. This field would couple to the structure and cause currents to flow.

In the thin-wire analysis, only the total current I(x) is computed. With a knowledge of I(x), one can easily calculate the total charge per unit length Q(x) along the wire from the continuity equation

$$- j\omega Q(x) = \frac{dI}{dx} . \tag{22a}$$

A time dependence of $e^{j\omega t}$ has been assumed and suppressed.

At an observation point x_o along the wing of the aircraft, the variation in the total charge per unit length in the longitudinal direction is postulated to be small so that locally the wing behaves like a two-dimensional airfoil with a net charge $Q(x_o)$. Substituting this value into Eq. (20) then determines the distribution of this charge over the circumference of the airfoil. From the continuity equation, it follows that the longitudinal surface current density J_ℓ on the airfoil has the same functional dependence in the transverse plane as the charge density σ_1. Thus, the current density on the aircraft wing may be expressed as

$$J(\theta) = \frac{I}{Q} \sigma_1(\theta). \tag{22b}$$

With the charge and current distributions along the circumference of the airfoil, it is then possible to estimate the strength of the local fields via the boundary conditions $\hat{n} \cdot \overline{E} = \sigma_1/\varepsilon_o$ and $\hat{n} \times \overline{H} = \overline{J}$.

V. Choice of the Parameters a, ℓ, w_o and α

With the Joukowski transformation, it is seen that there are four independent variables which describe the mapping of the circular contour C_a in the w plane into the airfoil in the z plane. In an actual airfoil, such as that shown in Fig. 2, it is noted that the length is greater than the thickness by about a factor 6. In addition, the trailing edge of the airfoil is rather pointed. With this information, it is possible to eliminate a large number of parameter choices which yield structures not resembling the physical airfoil.

For the airfoil to have a sharply pointed trailing end, it is seen from the nature of the transformation that the corresponding point on the circle C_a in the w plane should be as close as possible to one of the singular points at $w = \pm \ell$. As seen in Fig. 1a, this circle can actually pass through one singular point if $\alpha = 0$ and if $a = \ell + w_o$. If $w_o = 0$ such that the circle C_a coincides with the circle of radius ℓ, it is noted that both of the singularities are mapped onto the airfoil surface. For cases where $\alpha \neq 0$, it is seen that C_a can never touch the singular points since C_a is constrained to always lie outside the circle $|w| = \ell$. This implies that the trailing edge for this airfoil is not truely singular; it has a continuously turning normal derivative.

By imposing the condition that $a = \ell + w_o$ for the case when $\alpha \neq 0$, it can be seen from Fig. 1a that the circle C_a comes as close as possible to one of the singularities. This assures that for the other given parameters, the airfoil has the sharpest trailing edge possible.*

*With the Joukowski transformation, it is possible to consider airfoils which always exhibit a singular trailing edge. The forbidden region $|w| = \ell$, into which C_a must not enter, is not unique. In fact, any circle which intersects the points $w = \pm \ell$ can be thought of as defining a forbidden region. With such a redefinition of the forbidden region, it is possible to have the circle C_a always pass through one of the singular points, thereby giving rise to a singular edge on the airfoil. Unfortunately, the airfoils generated in this manner seem to have too much of a curve to them to realistically model an actual wing of an aircraft and this point has not been pursued.

With the constraint that $a = w_o + \ell$, the circle C_a maps into a thinner and thinner airfoil as w_o approaches 0. In the limit as $w_o = 0$, the airfoil becomes a plane. From this, it can be deduced that for relatively thin airfoils, the value of w_o should be small compared to ℓ. Hence, the best choices of w_o and ℓ for describing an airfoil lie within the range $0 < w_o < \ell < a$.

In considering the dependence of the airfoil shape on the angle α, it is seen that for $\alpha = 0^o$, the airfoil is singular at the trailing edge and is symmetric about the Re(z) axis. As α increases from 0^o the singularity at the trailing edge becomes less pronounced and the airfoil starts having a curve in it. At $\alpha = 90^o$, both the trailing and leading edges have the same shape, and the airfoil is symmetric about the Im(z) axis. As α increases even further, the airfoil takes the mirror image shape of the airfoil calculated for the angle $\pi - \alpha$. Thus, for actual airfoils, the values of α to be considered are given by $0 \leq \alpha \leq \pi/2$.

The final parameter that specifies the nature of the Joukowski airfoil is "a". This parameter defines the physical size of the airfoil. By normalizing the values of w_o and ℓ by the value "a" as done in Eq. (3), a normalized airfoil can be drawn in the z/a plane. The shape of this airfoil depends only on the parameters α and ℓ/a, since w_o/a is determined by the constraint $1 = w_o/a + \ell/a$. Once these parameters are decided upon so that the Joukowski airfoil is of the same approximate shape as the actual airfoil, the constant "a" may be found from the knowledge of the dimensions of the wing.

As an example of the method used to choose the parameters for this problem, consider the sample airfoil of Fig. 2. This is a typical cross section of the B-52 wing. By considering various values of α and ℓ/a, it was found that for $\alpha = 0$, $\ell/a = .87$ (which implies $w_o/a = .13$), the normalized shape of the Joukowski airfoil is close to that of the actual wing. The normalized airfoil for this case is shown in Fig. 5a.

From Fig. 2, it is noted that the overall linear dimensions of the actual airfoil is 8.5 meters. Noting that this corresponds to a normalized length of $x/a = 3.55$ in Fig. 5a, it is readily calculated that the radius of circle C_a is to be $a = 8.5/3.55 = 2.39$ meters.

It is interesting to consider the significance of the parameter "a",

which defines the radius of the circle C_a in the w plane. As is well known from the theory of conformal mapping, the total charge per unit length on the cylinder in the w plane is equal to the total charge per unit length on the airfoil in the w plane. Similarly, the potentials of both structures are the same. As a result, the capacitance per unit length of the airfoil is identical to that of a right circular cylinder of radius "a" This value "a" is defined as the equivalent radius of the airfoil, and may be determined by the method indicated above.

In using a thin-wire structure to model an actual aircraft, it is necessary to specify the radius of the wire elements. The most logical choice is to choose the radius such that the capacitance per unit length of the wire is equal to that of the aircraft. This implies that for modeling the airfoils on an aircraft, the parameter "a" should be used as the wire radius.

Since the cross section of the actual aircraft wing is not constant along its length, the wire radius for the thin-wire model should be tapered to account for this effect. By applying the above procedure for determining the effective radius "a" at various points along the wing, the nature of the desired taper in the wing elements for the thin-wire model can be found.

VI. Numerical Results

Employing the analysis technique described in the previous sections, the charge distribution on various airfoils has been determined. In addition to the airfoil shapes, data is presented for a few other simple obstacles, such as a flat plate, ellipses and a circle, which are also generated by the Joukowski transformation. Since the problem of the airfoil immersed in the static electric field is so simply related to the problem of the charged airfoil, only data for this latter case is presented. The behavior of the airfoil in the electrostatic field may then be calculated by a simple multiplication by the cosine factor indicated in Eq. (21). This cosine function is plotted along with each of the charge density curves for two values of θ_{inc}, 0^{o} and 90^{o}, so as to indicate what the multiplicative term should be. The only exception to this is Fig. 8 which shows the induced charge on the $\alpha = 0^{o}$ airfoil of Fig. 5a with $\theta_{inc} = 0^{o}$ and 90^{o}. This airfoil most closely resembles the B-52 airfoil in Fig. 2 and is presented so the reader can see the general shape of the charge distribution in these problems.

Figures 3a and 3b show the flat plate, ellipses and the circle generated by the transformation. For these figures, $\alpha = 0$, $w_o/a = 0$ and ℓ/a varies between 1 to 0. Figure 3c presents the normalized charged distribution on these structures as a function of the angle θ in the w plane. These points correspond to the non-uniformily spaced points as indicated on the surfaces of the obstacles. Table 1 gives, as a function of θ, the magnitude and angle of the normalized quantity z/a which defines the surface of the obstacle.

For these obstacles, it is readily seen that the charge tends to collect near the sharply curved portions of the surface. For the flat plate where $\ell/a = 1.0$, the charge density is actually infinite at the singular edge. The variation of the charge density at the positions $\theta = 0^{o}$ and $\theta = 90^{o}$ on these symmetric structures is presented in Fig. 3d as a function of the parameter ℓ/a. In some cases, the ellipse might be an adequate approximation to the cross section of the fuselage of an aircraft and these results may be employed in a study of this portion of the aircraft.

In a similar manner, Figs. 4a through 7a present the numerical results for various airfoil-like structures. Each figure contains four seperate

airfoils having fixed ℓ/a and w_o/a values, but varying values of α. Tables 2 through 5 give the normalized co-ordinates of the airfoils. The corresponding plots of the charge density on the airfoils are presented in Figs. 4b through 7b.

Figures 9a and 9b summarize the behavior of the charge on the airfoil as the parameter α is varied. The charge density on the leading and trailing edges of the airfoil is plotted as a function of α for various values of ℓ/a. The value of σ on the trailing edge of the airfoil is infinite for $\alpha = 0$, but for other values of α, a finite value is computed. Note that the charge density on the trailing edge of the airfoil is plotted on a logarithmic scale.

For an airfoil immersed in an incident electric field, it is evident that there must be two positions on the airfoil where there is a null in the induced charge density. Figures 10a and 10b show, as a function of the parameter α, the angle of incidence of the electric field which causes a null in the charge distribution in the leading and trailing edges of the airfoil. This is on the left scale.

For the cases where $\alpha \neq 0$, the positions of the trailing edges (and also the leading edges) are not sharply defined due to the non-singular nature of the airfoil. In these cases, the location of the trailing and leading edges was defined as being that point where the derivative dz/dw took on a maximum value.

From Figs. 10a and 10b it is possible to determine the value of θ_o which corresponds to the leading or trailing edge of the airfoil. From the simple cosine dependence on the induced charge density it is readily seen that the position of these edges are given by

$$\theta_o = \theta_{inc} - 90^o.$$

This angle defining the leading or trailing edges of the airfoils may be read off the scale on the right hand side of Figs. 10a and 10b.

VII. Conclusion

Through the use of a conformal mapping technique, which maps a circle into an airfoil shape, expressions for the charge density on the airfoil located in an electrostatic field are derived and related to the charge density on the same airfoil having a net charge.

The results of numerical calculations for some typical airfoil structures are presented, showing not only the airfoil shape, but the charge distributions for the airfoils having a net charge. Summary curves are presented showing how the charge density at the leading and trailing edges of the airfoil behave as a function of the airfoil shape.

By using the results of a thin-wire analysis to compute the total charge induced on the aircraft wing, it is possible to approximate the charge distribution on the wing of an actual aircraft subject to an EMP. Although the transformation as employed in this note is primarily intended for the study of airfoils, such a technique could be used to describe the behavior of charge on a fuselage of an aircraft which has an elliptical cross section.

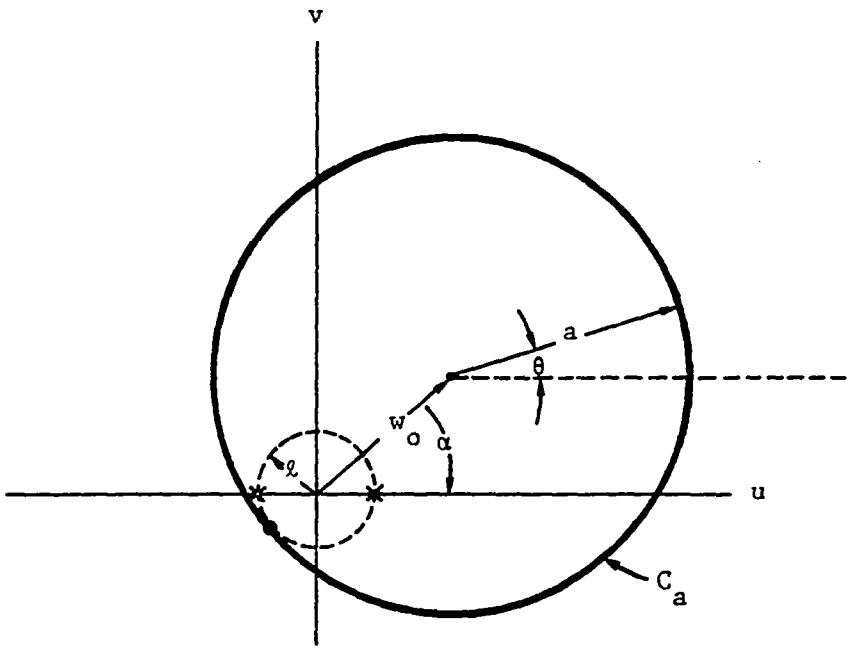

w plane

Figure 1a. The circle C_a in the complex w plane which maps into the airfoil in the z plane.

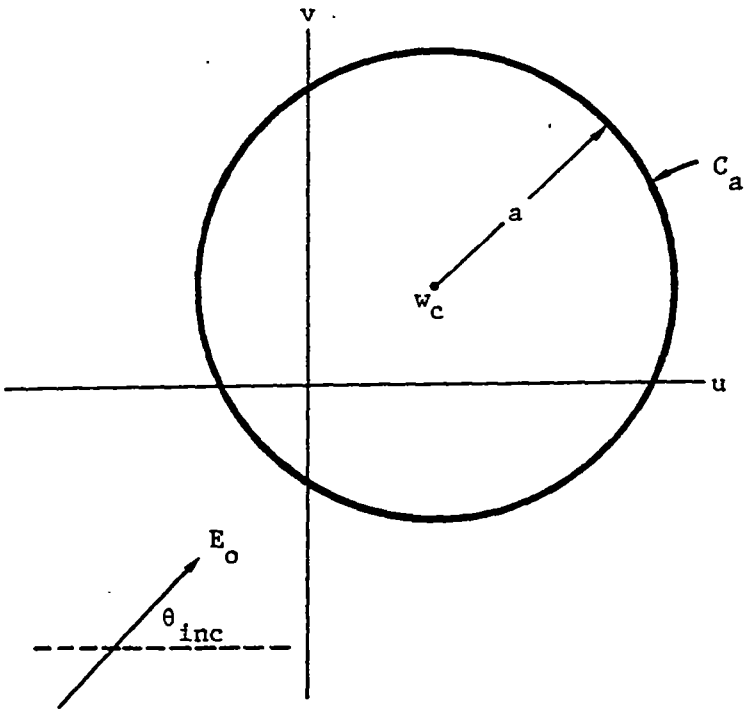

Figure 1b. Definition of the angle of incidence θ_{inc} of the electric field falling on C_a.

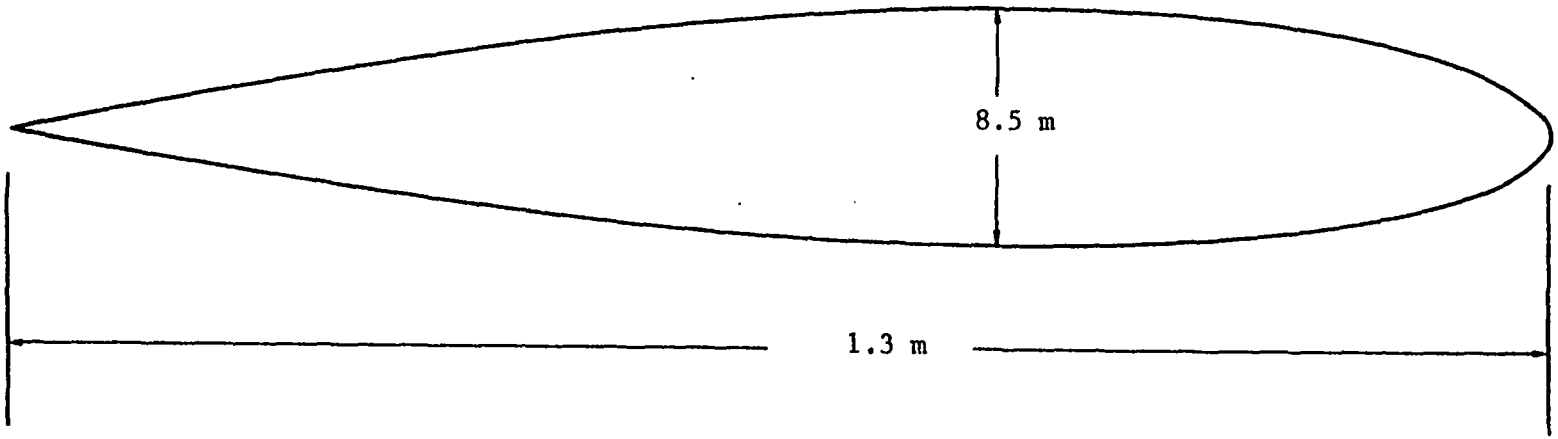

Figure 2. The approximate shape of the airfoil of a B-52 at a position near the junction of the wing and fuselage of the aircraft.

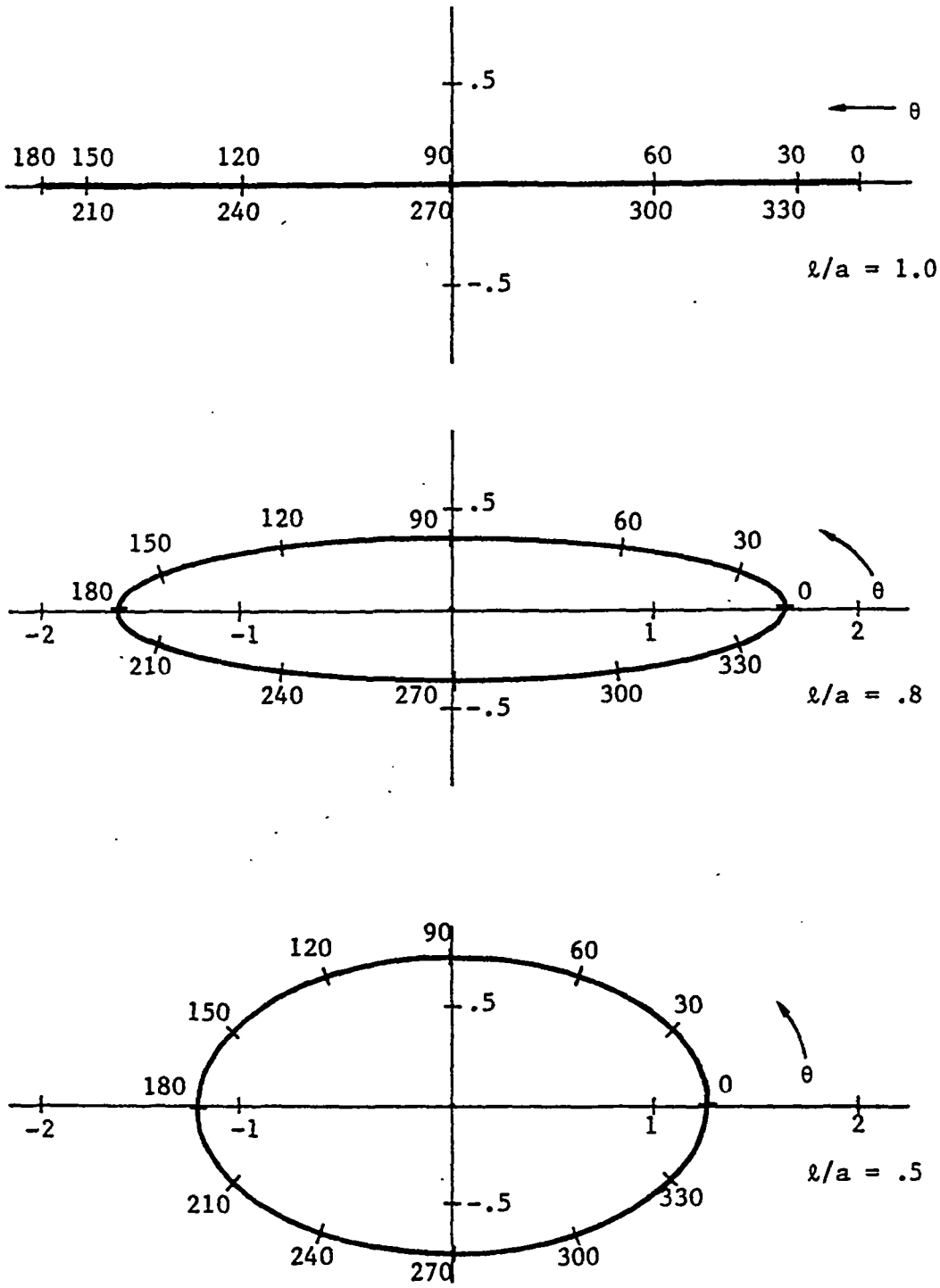

Figure 3a. Shapes of ellipses generated by the Joukowski transformation for $w_o/a = 0$, $\alpha = 0$ and a fixed value of ℓ.

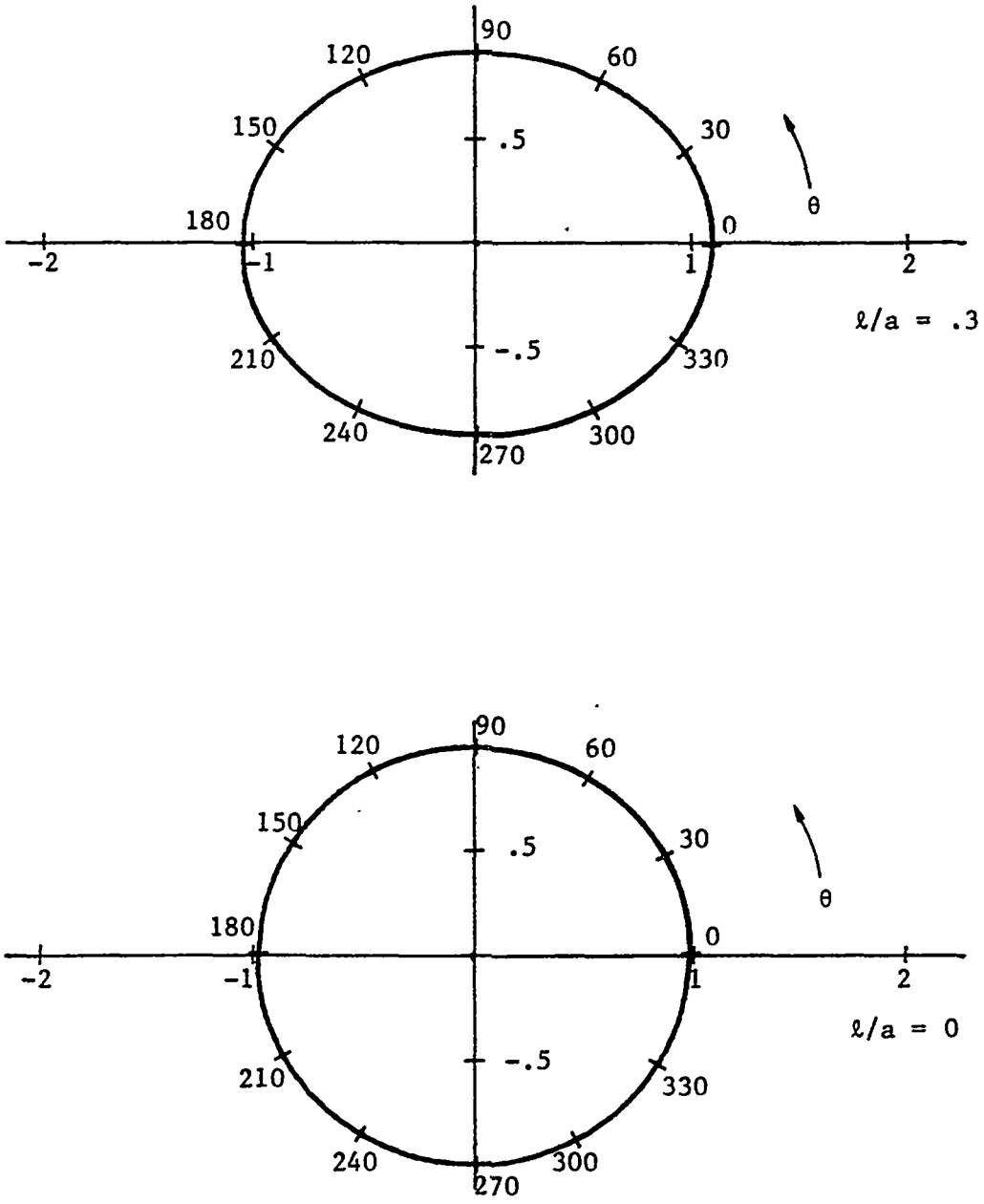

Figure 3b. Shapes of ellipses generated by the Joukowski transformation for $w_o/a = 0$, $\alpha = 0$ and a fixed value of ℓ.

Table 1

Normalized Ellipses as a Function of the Parameter θ

$w_o/a = 0.0$, $\alpha = 0.0$

	ℓ/a = 1.0		ℓ/a = .8		ℓ/a = .5		ℓ/a = .3		ℓ/a = 0.0	
θ	|z/a|	Ang(z)	|z/a|	Ang(z)	|z/a|	Ang(z)	|z/a|	Ang(z)	|z/a|	Ang(z)
0°	2.00	0.00°	1.64	0.00°	1.25	0.00°	1.09	0.00°	1.00	0.00°
10°	1.97	0.00°	1.62	2.22°	1.24	6.04°	1.09	8.37°	1.00	10.00°
20°	1.88	0.00°	1.55	4.57°	1.20	12.32°	1.07	16.90°	1.00	20.00°
30°	1.73	0.00°	1.43	7.22°	1.15	19.11°	1.05	25.73°	1.00	30.00°
40°	1.53	0.00°	1.28	10.44°	1.07	26.72°	1.02	35.01°	1.00	40.00°
50°	1.29	0.00°	1.09	14.66°	0.99	35.57°	0.99	44.85°	1.00	50.00°
60°	1.00	0.00°	0.88	20.82°	0.90	46.10°	0.96	55.33°	1.00	60.00°
70°	0.68	0.00°	0.66	31.09°	0.82	58.76°	0.93	66.44°	1.00	70.00°
80°	0.35	0.00°	0.45	51.23°	0.77	73.62°	0.92	78.07°	1.00	80.00°
90°	0.00	0.00°	0.36	90.00°	0.75	90.00°	0.91	90.00°	1.00	90.00°
100°	0.35	180.00°	0.45	128.77°	0.77	106.38°	0.92	101.93°	1.00	100.00°
110°	0.68	180.00°	0.66	148.91°	0.82	121.24°	0.93	113.56°	1.00	110.00°
120°	1.00	180.00°	0.88	159.18°	0.90	133.90°	0.96	124.67°	1.00	120.00°
130°	1.29	180.00°	1.09	165.34°	0.99	144.43°	0.99	135.15°	1.00	130.00°
140°	1.53	180.00°	1.28	169.56°	1.07	153.28°	1.02	144.99°	1.00	140.00°
150°	1.73	180.00°	1.43	172.78°	1.15	160.89°	1.05	154.27°	1.00	150.00°
160°	1.88	180.00°	1.55	175.43°	1.20	167.68°	1.07	163.10°	1.00	160.00°
170°	1.97	180.00°	1.62	177.78°	1.24	173.96°	1.09	171.63°	1.00	170.00°
180°	2.00	180.00°	1.64	180.00°	1.25	180.00°	1.09	180.00°	1.00	180.00°
190°	1.97	180.00°	1.62	182.22°	1.24	186.04°	1.09	188.37°	1.00	190.00°
200°	1.88	180.00°	1.55	184.57°	1.20	192.32°	1.07	196.90°	1.00	200.00°
210°	1.73	180.00°	1.43	187.22°	1.15	199.11°	1.05	205.73°	1.00	210.00°
220°	1.53	180.00°	1.28	190.44°	1.07	206.72°	1.02	215.01°	1.00	220.00°
230°	1.29	180.00°	1.09	194.66°	0.99	215.57°	0.99	224.85°	1.00	230.00°
240°	1.00	180.00°	0.88	200.82°	0.90	226.10°	0.96	235.33°	1.00	240.00°
250°	0.68	180.00°	0.66	211.09°	0.82	238.76°	0.93	246.44°	1.00	250.00°
260°	0.35	180.00°	0.45	231.23°	0.77	253.62°	0.92	258.07°	1.00	260.00°
270°	0.00	360.00°	0.36	270.00°	0.75	270.00°	0.91	270.00°	1.00	270.00°
280°	0.35	360.00°	0.45	308.77°	0.77	286.38°	0.92	281.93°	1.00	280.00°
290°	0.68	360.00°	0.66	328.91°	0.82	301.24°	0.93	293.56°	1.00	290.00°
300°	1.00	360.00°	0.88	339.18°	0.90	313.90°	0.96	304.67°	1.00	300.00°
310°	1.29	360.00°	1.09	345.34°	0.99	324.43°	0.99	315.15°	1.00	310.00°
320°	1.53	360.00°	1.28	349.56°	1.07	333.28°	1.02	324.99°	1.00	320.00°
330°	1.73	360.00°	1.43	352.78°	1.15	340.89°	1.05	334.27°	1.00	330.00°
340°	1.88	360.00°	1.55	355.43°	1.20	347.68°	1.07	343.10°	1.00	340.00°
350°	1.97	360.00°	1.62	357.78°	1.24	353.96°	1.09	351.63°	1.00	350.00°
360°	2.00	360.00°	1.64	360.00°	1.25	360.00°	1.09	360.00°	1.00	360.00°

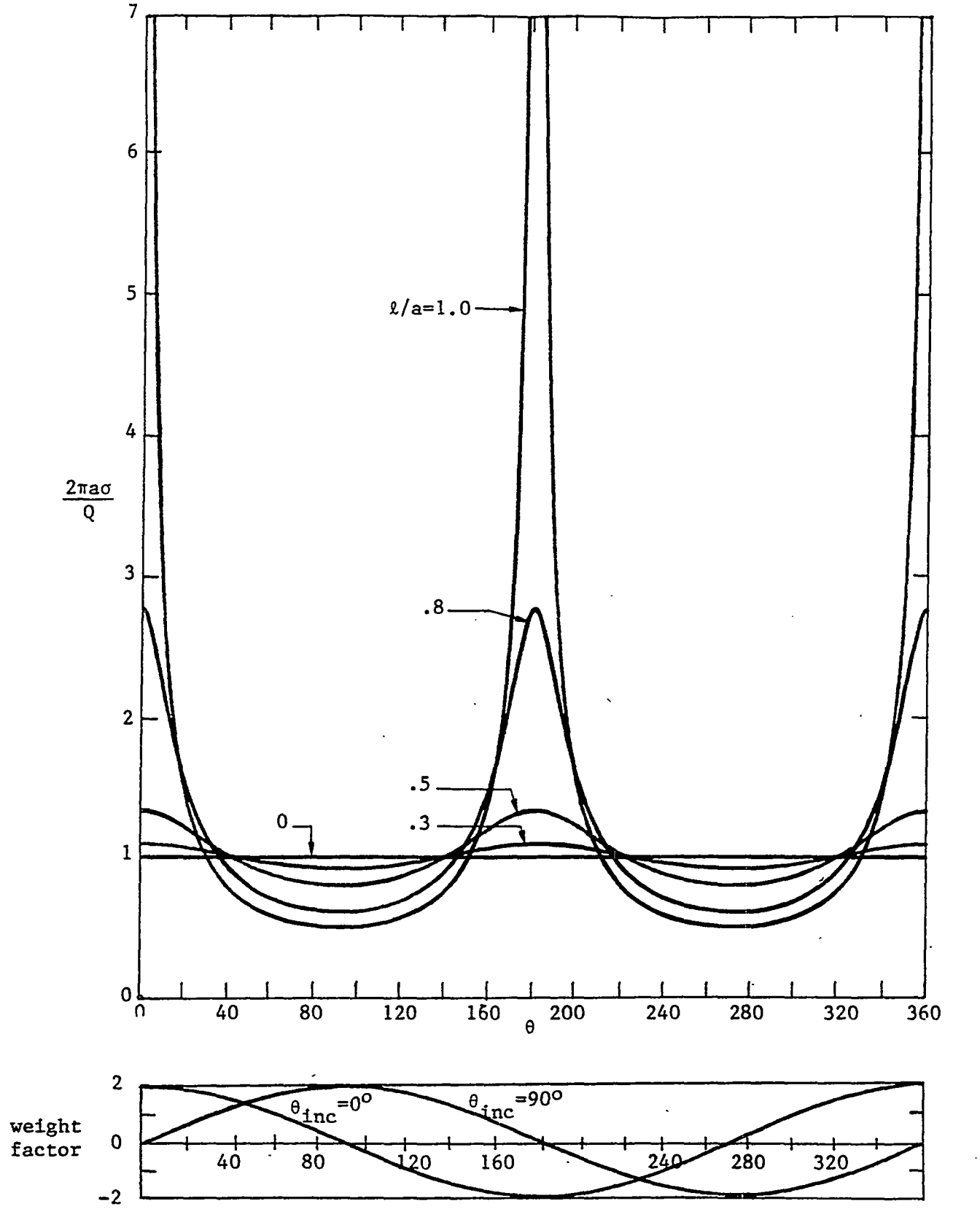

Figure 3c. The surface charge density, shown as a function of position, on the ellipses of Figures 3a and 3b having a net charge per unit length of Q. The weight factors for determining the induced surface charge when a static electric field is incident at $\theta_{inc} = 0^o$ and 90^o are also given.

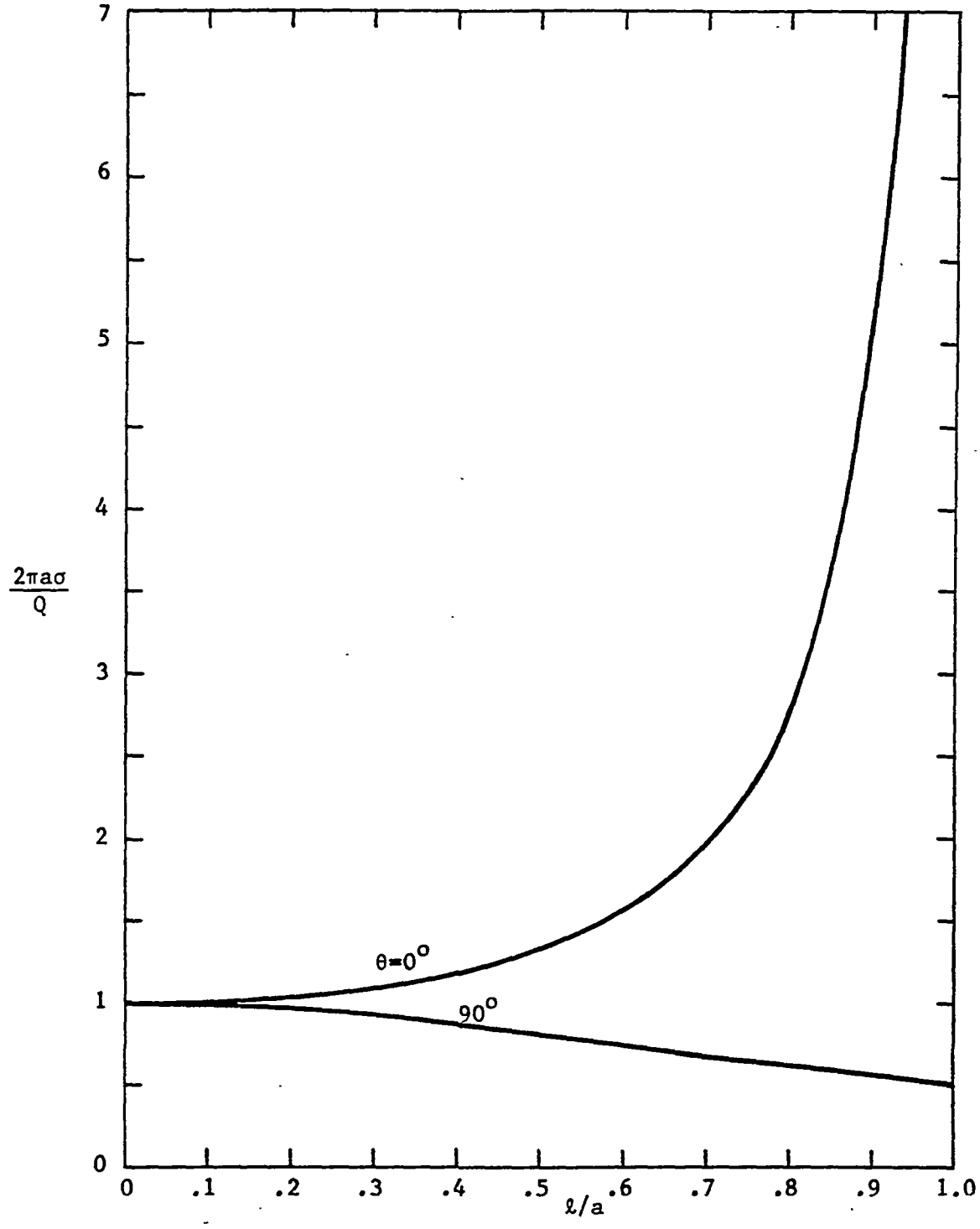

Figure 3d. Plot of the normalized charge density at $\theta = 0^{\circ}$ and 90° on the ellipses of Figures 3a and 3b, shown as a function of the parameter ℓ/a.

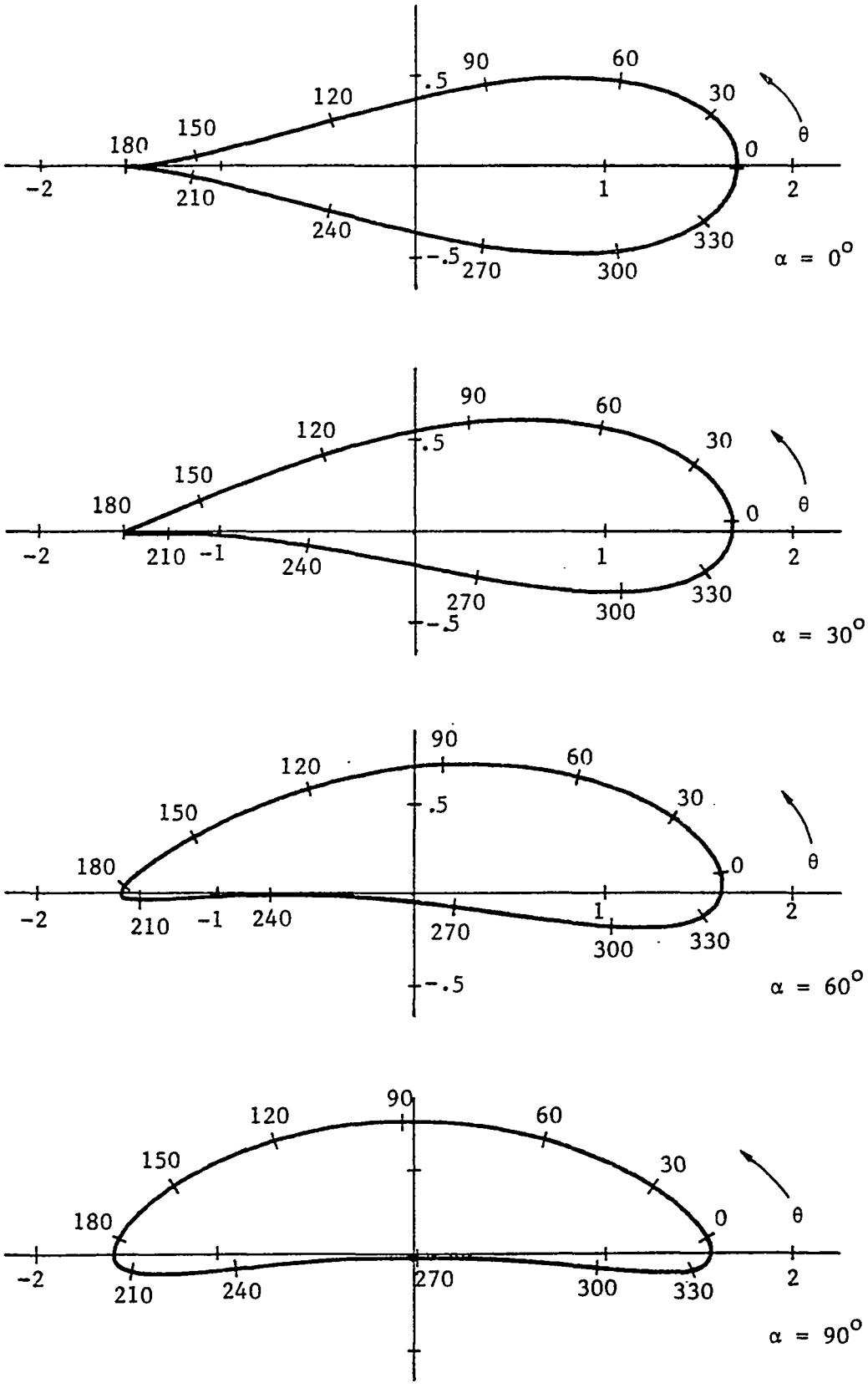

Figure 4a. Shapes of normalized airfoils defined by $\ell/a = .77$, $w_o/a = .23$ and the parameter α.

Table 2

Normalized Airfoils as a Function of the Parameter θ

$\ell/a = .77$, $w_o/a = .23$

	$\alpha = 0^o$		$\alpha = 30^o$		$\alpha = 60^o$		$\alpha = 90^o$	
θ	$\lvert z/a \rvert$	Ang(z)	$\lvert z/a \rvert$	Ang(z)	$\lvert z/a \rvert$	Ang(z)	$\lvert z/a \rvert$	Ang(z)
0^o	1.71	0.00^o	1.69	2.31^o	1.63	3.76^o	1.57	3.68^o
10^o	1.70	3.56^o	1.67	5.98^o	1.60	7.52^o	1.51	7.31^o
20^o	1.65	7.16^o	1.61	9.90^o	1.53	11.78^o	1.43	11.77^o
30^o	1.57	10.84^o	1.53	14.16^o	1.44	16.66^o	1.33	17.23^o
40^o	1.46	14.70^o	1.42	18.86^o	1.33	22.31^o	1.21	23.92^o
50^o	1.33	18.86^o	1.29	24.19^o	1.21	28.99^o	1.08	32.21^o
60^o	1.16	23.58^o	1.14	30.51^o	1.07	37.12^o	0.96	42.63^o
70^o	0.98	29.35^o	0.98	38.39^o	0.94	47.31^o	0.85	55.75^o
80^o	0.77	37.35^o	0.82	48.95^o	0.82	60.41^o	0.78	71.81^o
90^o	0.57	50.55^o	0.67	64.10^o	0.73	77.14^o	0.75	90.00^o
100^o	0.40	76.74^o	0.56	86.12^o	0.69	96.95^o	0.78	108.19^o
110^o	0.37	120.38^o	0.55	113.41^o	0.72	117.12^o	0.85	124.25^o
120^o	0.52	152.48^o	0.64	137.65^o	0.80	134.50^o	0.96	137.37^o
130^o	0.75	167.27^o	0.79	154.26^o	0.93	147.95^o	1.08	147.79^o
140^o	0.99	174.30^o	0.98	164.79^o	1.07	157.97^o	1.21	156.08^o
150^o	1.21	177.78^o	1.16	171.48^o	1.21	165.41^o	1.33	162.77^o
160^o	1.39	179.37^o	1.32	175.70^o	1.34	170.95^o	1.43	168.23^o
170^o	1.50	179.92^o	1.45	178.25^o	1.45	175.02^o	1.51	172.69^o
180^o	1.54	180.00^o	1.53	179.59^o	1.52	177.91^o	1.57	176.32^o
190^o	1.50	180.08^o	1.54	180.10^o	1.55	179.80^o	1.59	179.20^o
200^o	1.39	180.63^o	1.47	180.10^o	1.52	180.83^o	1.56	181.39^o
210^o	1.21	182.22^o	1.33	180.00^o	1.43	181.13^o	1.49	182.90^o
220^o	0.99	185.70^o	1.13	180.31^o	1.27	180.89^o	1.37	183.75^o
230^o	0.75	192.73^o	0.87	181.92^o	1.05	180.36^o	1.19	183.97^o
240^o	0.52	207.52^o	0.58	187.03^o	0.77	180.00^o	0.95	183.60^o
250^o	0.37	239.62^o	0.29	205.66^o	0.45	181.09^o	0.67	182.72^o
260^o	0.40	283.26^o	0.19	283.56^o	0.12	197.03^o	0.35	181.46^o
270^o	0.57	309.45^o	0.42	324.18^o	0.23	341.02^o	0.00	270.00^o
280^o	0.77	322.65^o	0.69	334.62^o	0.55	347.24^o	0.35	358.54^o
290^o	0.98	330.65^o	0.93	339.70^o	0.83	348.84^o	0.67	357.28^o
300^o	1.16	336.42^o	1.14	343.29^o	1.07	350.01^o	0.95	356.40^o
310^o	1.33	341.14^o	1.32	346.40^o	1.27	351.35^o	1.19	356.03^o
320^o	1.46	345.30^o	1.46	349.40^o	1.43	353.03^o	1.37	356.25^o
330^o	1.57	349.16^o	1.57	352.43^o	1.54	355.10^o	1.49	357.10^o
340^o	1.65	352.84^o	1.64	355.56^o	1.61	357.57^o	1.56	358.61^o
350^o	1.70	356.44^o	1.68	358.85^o	1.64	0.46^o	1.59	0.80^o
360	1.71	360.00^o	1.69	2.31^o	1.63	3.76^o	1.57	3.68^o

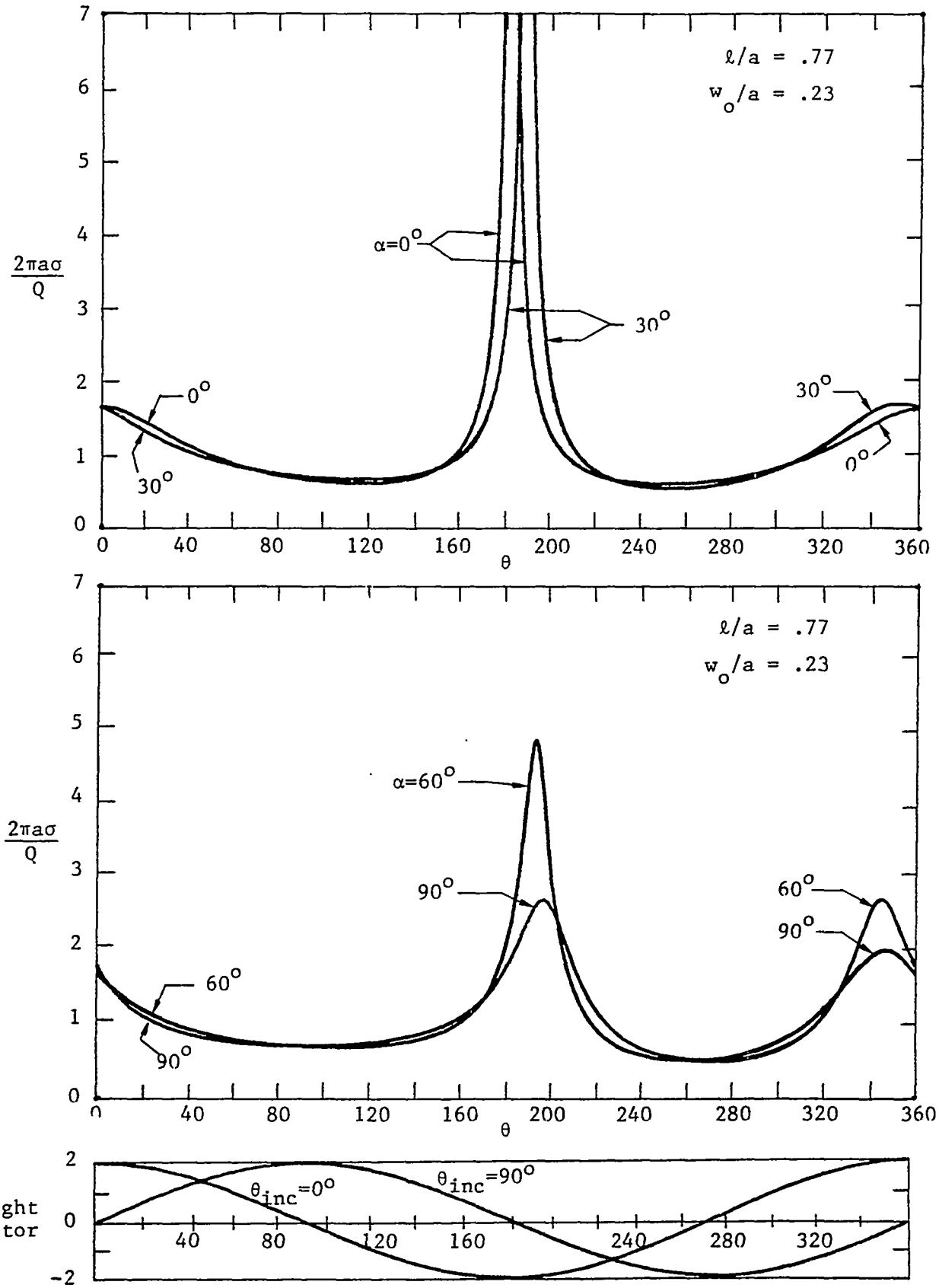

Figure 4b. The charge density on the airfoils of Figure 4a having a net charge Q per unit length shown as a function of position. Weight functions for determining the induced surface charge due to an electric field incident on the airfoil at an angle θ_{inc} are also given.

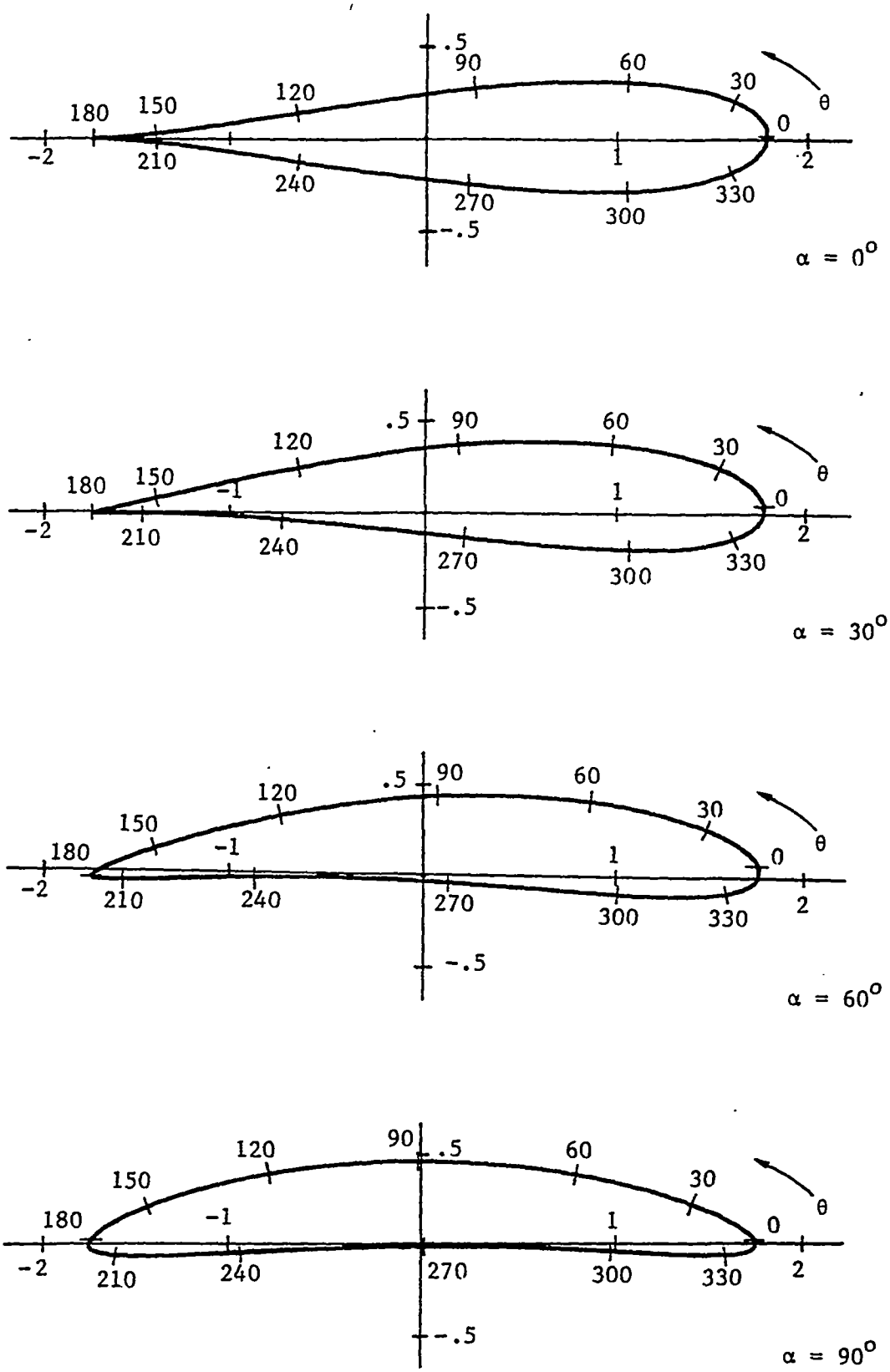

Figure 5a. Shapes of normalized airfoils defined by $\ell/a = .87$, $w_o/a = .13$, and the parameter α.

Table 3

Normalized Airfoils as a Function of the Parameter θ

$\ell/a = .87$, $w_o/a = .13$

	$\alpha = 0^o$		$\alpha = 30^o$		$\alpha = 60^o$		$\alpha = 90^o$	
θ	|z/a|	Ang(z)	|z/a|	Ang(z)	|z/a|	Ang(z)	|z/a|	Ang(z)
0^o	1.80	360.00^o	1.79	0.81^o	1.77	1.24^o	1.74	1.09^o
10^o	1.78	2.28^o	1.76	3.11^o	1.72	3.43^o	1.69	2.96^o
20^o	1.72	4.57^o	1.69	5.62^o	1.64	6.01^o	1.59	5.38^o
30^o	1.61	6.95^o	1.58	8.40^o	1.52	9.07^o	1.45	8.48^o
40^o	1.47	9.48^o	1.43	11.57^o	1.36	12.80^o	1.29	12.52^o
50^o	1.30	12.31^o	1.25	15.37^o	1.18	17.52^o	1.10	17.97^o
60^o	1.09	15.73^o	1.05	20.25^o	0.98	23.89^o	0.89	25.80^o
70^o	0.85	20.45^o	0.83	27.22^o	0.78	33.32^o	0.69	38.01^o
80^o	0.59	28.55^o	0.60	38.91^o	0.58	48.97^o	0.53	58.50^o
90^o	0.34	48.43^o	0.41	62.70^o	0.45	76.47^o	0.46	90.00^o
100^o	0.23	109.63^o	0.35	107.25^o	0.45	113.05^o	0.53	121.50^o
110^o	0.42	155.77^o	0.49	143.70^o	0.59	140.11^o	0.69	141.99^o
120^o	0.70	169.51^o	0.72	160.60^o	0.80	155.26^o	0.89	154.20^o
130^o	0.97	175.06^o	0.96	168.98^o	1.01	164.10^o	1.10	162.03^o
140^o	1.23	177.76^o	1.19	173.72^o	1.22	169.75^o	1.29	167.48^o
150^o	1.44	179.12^o	1.40	176.61^o	1.41	173.60^o	1.45	171.52^o
160^o	1.60	179.75^o	1.56	178.37^o	1.56	176.30^o	1.59	174.62^o
170^o	1.71	179.97^o	1.68	179.39^o	1.67	178.19^o	1.69	177.04^o
180^o	1.74	180.00^o	1.74	179.91^o	1.73	179.45^o	1.74	178.91^o
190^o	1.71	180.03^o	1.73	180.07^o	1.74	180.22^o	1.75	180.32^o
200^o	1.60	180.25^o	1.65	180.05^o	1.68	180.58^o	1.71	181.31^o
210^o	1.44	180.88^o	1.51	180.00^o	1.57	180.62^o	1.61	181.94^o
220^o	1.23	182.24^o	1.30	180.13^o	1.39	180.44^o	1.45	182.22^o
230^o	0.97	184.94^o	1.05	180.78^o	1.15	180.17^o	1.24	182.19^o
240^o	0.70	190.49^o	0.76	182.66^o	0.87	180.00^o	0.98	181.90^o
250^o	0.42	204.23^o	0.45	188.38^o	0.55	180.45^o	0.68	181.39^o
260^o	0.23	250.37^o	0.15	221.05^o	0.22	184.70^o	0.35	180.73^o
270^o	0.34	311.57^o	0.25	326.70^o	0.13	342.93^o	0.00	270.00^o
280^o	0.59	331.45^o	0.55	341.93^o	0.46	351.96^o	0.35	359.27^o
290^o	0.85	339.55^o	0.83	346.55^o	0.77	353.30^o	0.68	358.61^o
300^o	1.09	344.27^o	1.09	349.15^o	1.05	353.98^o	0.98	358.10^o
310^o	1.30	347.69^o	1.31	351.15^o	1.29	354.64^o	1.25	357.81^o
320^o	1.47	350.52^o	1.49	352.98^o	1.48	355.47^o	1.45	357.78^o
330^o	1.61	353.05^o	1.63	354.80^o	1.63	356.51^o	1.61	358.06^o
340^o	1.72	355.43^o	1.73	356.68^o	1.72	357.81^o	1.71	358.69^o
350^o	1.78	357.73^o	1.78	358.68^o	1.77	359.38^o	1.75	359.68^o
360^o	1.80	360.00^o	1.79	0.81^o	1.77	1.24^o	1.74	1.09^o

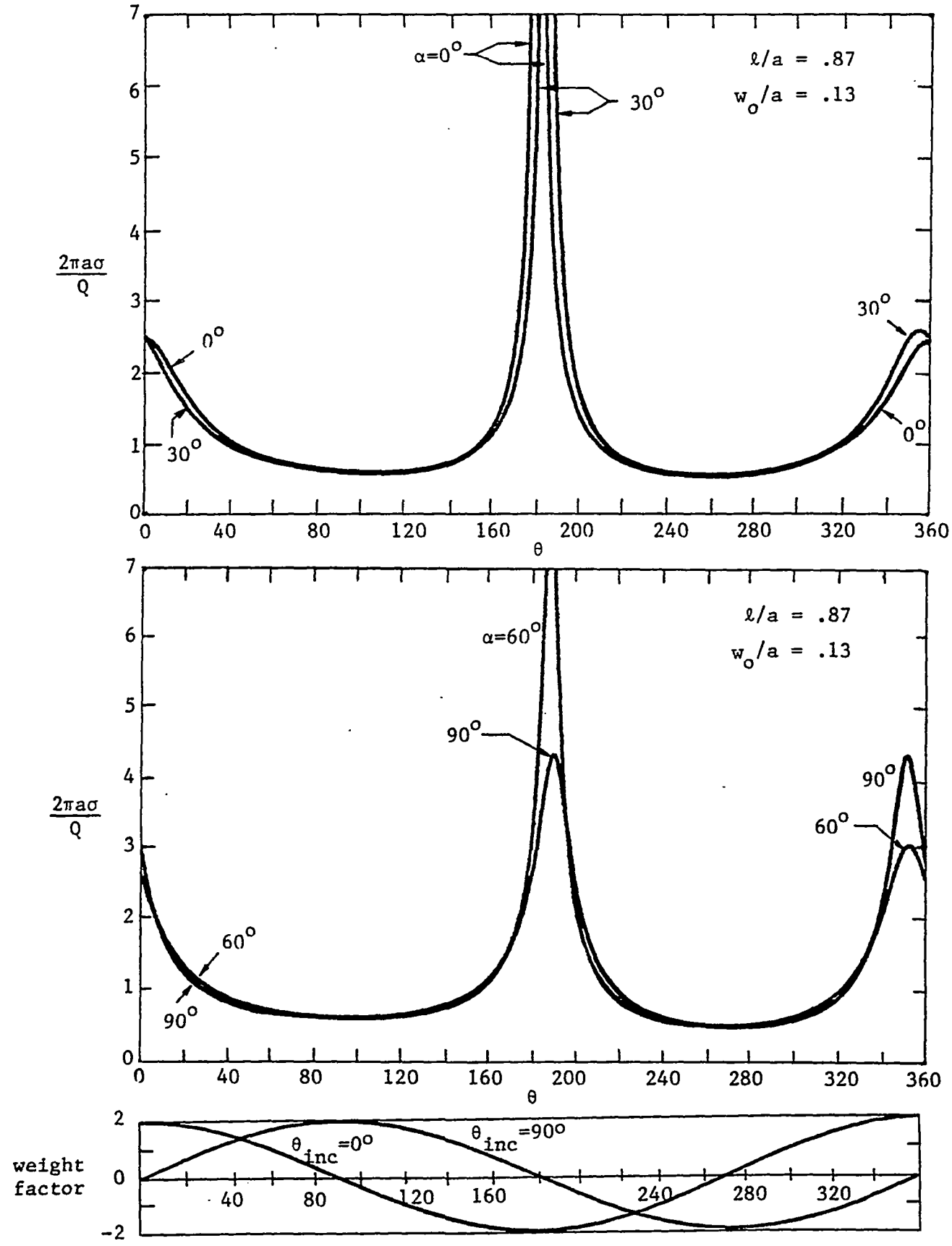

Figure 5b. The charge density on the airfoils of Figure 5a having a net charge Q per unit length, shown as a function of position. Weight functions for determining the induced surface charge due to an electric field incident on the airfoil at an angle θ_{inc} are also given.

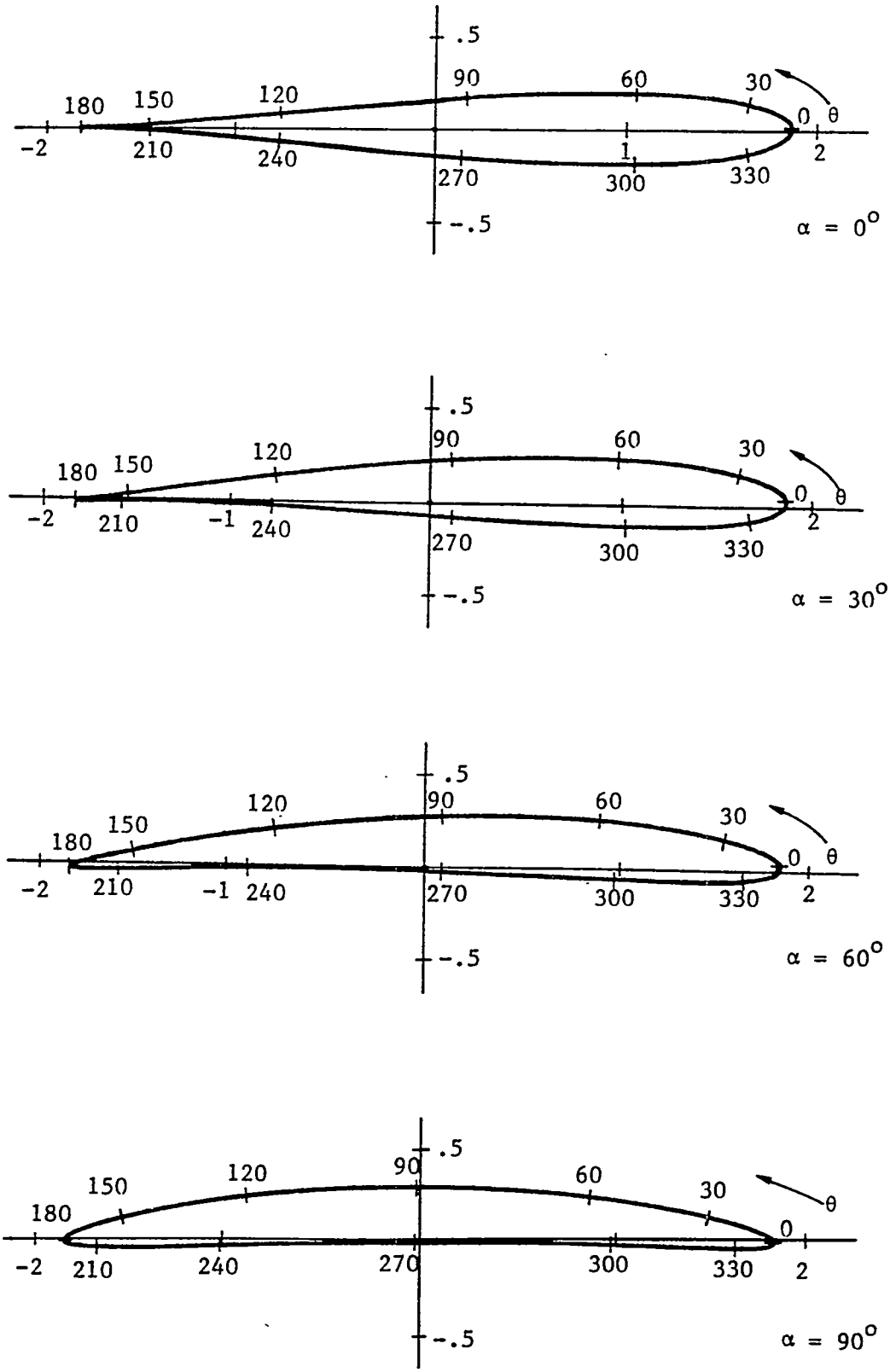

Figure 6a. Shapes of normalized airfoils defined by $\ell/a = .92$, $w_o/a = .08$ and the parameter α.

Table 4

Normalized Airfoils as a Function of the Parameter θ

$\ell/a = .92$, $w_o/a = .08$

	$\alpha = 0^o$		$\alpha = 30^o$		$\alpha = 60^o$		$\alpha = 90^o$	
θ	|z/a|	Ang(z)	|z/a|	Ang(z)	|z/a|	Ang(z)	|z/a|	Ang(z)
0^o	1.86	360.00^o	1.86	0.32^o	1.85	0.47^o	1.84	0.40^o
10^o	1.84	1.48^o	1.83	1.80^o	1.81	1.82^o	1.79	1.47^o
20^o	1.77	2.97^o	1.75	3.42^o	1.72	3.44^o	1.69	2.89^o
30^o	1.65	4.53^o	1.62	5.24^o	1.58	5.38^o	1.55	4.75^o
40^o	1.49	6.20^o	1.45	7.36^o	1.41	7.79^o	1.36	7.23^o
50^o	1.29	8.11^o	1.25	9.95^o	1.20	10.94^o	1.14	10.66^o
60^o	1.05	10.50^o	1.02	13.42^o	0.97	15.40^o	0.90	15.84^o
70^o	0.78	14.07^o	0.76	18.82^o	0.71	22.65^o	0.65	24.79^o
80^o	0.49	21.19^o	0.49	29.55^o	0.47	37.39^o	0.42	44.09^o
90^o	0.22	47.19^o	0.26	61.79^o	0.29	75.99^o	0.30	90.00^o
100^o	0.22	142.70^o	0.28	132.14^o	0.35	131.55^o	0.42	135.91^o
110^o	0.51	168.14^o	0.53	160.27^o	0.58	155.82^o	0.65	155.21^o
120^o	0.81	174.68^o	0.81	169.70^o	0.84	165.83^o	0.90	164.16^o
130^o	1.09	177.45^o	1.08	174.19^o	1.10	171.13^o	1.14	169.34^o
140^o	1.34	178.84^o	1.32	176.72^o	1.33	174.41^o	1.36	172.77^o
150^o	1.55	179.54^o	1.53	178.25^o	1.52	176.59^o	1.55	175.25^o
160^o	1.71	179.87^o	1.69	179.18^o	1.68	178.20^o	1.69	177.11^o
170^o	1.81	179.98^o	1.79	179.71^o	1.79	179.14^o	1.79	178.53^o
180^o	1.84	180.00^o	1.84	179.97^o	1.84	179.81^o	1.84	179.60^o
190^o	1.81	180.02^o	1.82	180.05^o	1.83	180.21^o	1.84	180.39^o
200^o	1.71	180.13^o	1.74	180.03^o	1.76	180.38^o	1.78	180.94^o
210^o	1.55	180.46^o	1.59	180.00^o	1.63	180.37^o	1.66	181.25^o
220^o	1.34	181.16^o	1.39	180.07^o	1.44	180.26^o	1.48	181.37^o
230^o	1.09	182.55^o	1.14	180.41^o	1.20	180.09^o	1.26	181.32^o
240^o	0.81	185.32^o	0.85	181.37^o	0.92	180.00^o	0.99	181.13^o
250^o	0.51	191.86^o	0.54	184.09^o	0.60	180.24^o	0.68	180.82^o
260^o	0.22	217.30^o	0.21	196.47^o	0.27	182.22^o	0.35	180.43^o
270^o	0.22	312.81^o	0.16	327.98^o	0.08	343.78^o	0.00	270.00^o
280^o	0.49	338.81^o	0.47	347.17^o	0.42	354.70^o	0.35	359.57^o
290^o	0.78	345.93^o	0.78	351.00^o	0.74	355.74^o	0.68	359.18^o
300^o	1.05	349.50^o	1.06	352.86^o	1.04	356.19^o	0.99	358.87^o
310^o	1.29	351.89^o	1.30	354.19^o	1.29	356.58^o	1.26	358.68^o
320^o	1.49	353.80^o	1.51	355.36^o	1.51	357.05^o	1.48	358.63^o
330^o	1.65	355.47^o	1.67	356.51^o	1.67	357.65^o	1.66	358.75^o
340^o	1.77	357.03^o	1.78	357.70^o	1.78	358.41^o	1.78	359.06^o
350^o	1.84	358.52^o	1.84	358.96^o	1.84	359.34^o	1.84	359.61^o
360^o	1.86	360.00^o	1.86	0.32^o	1.85	0.47^o	1.84	0.40^o

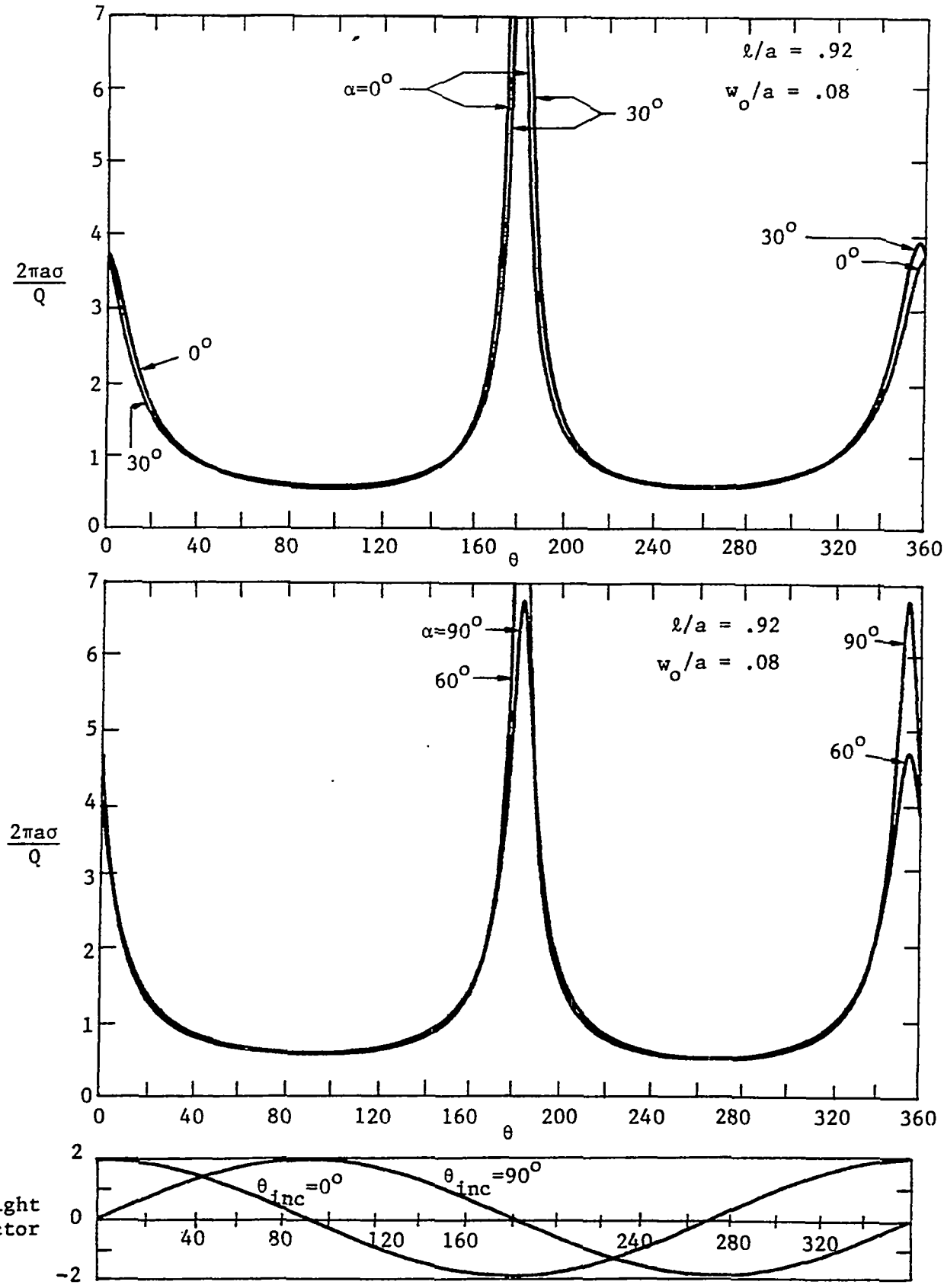

Figure 6b. The charge density on the airfoils of Figure 6a having a net charge Q per unit length, shown as a function of position. Weight functions for determining the induced surface charge due to an electric field incident on the airfoil at an angle θ_{inc} are also given.

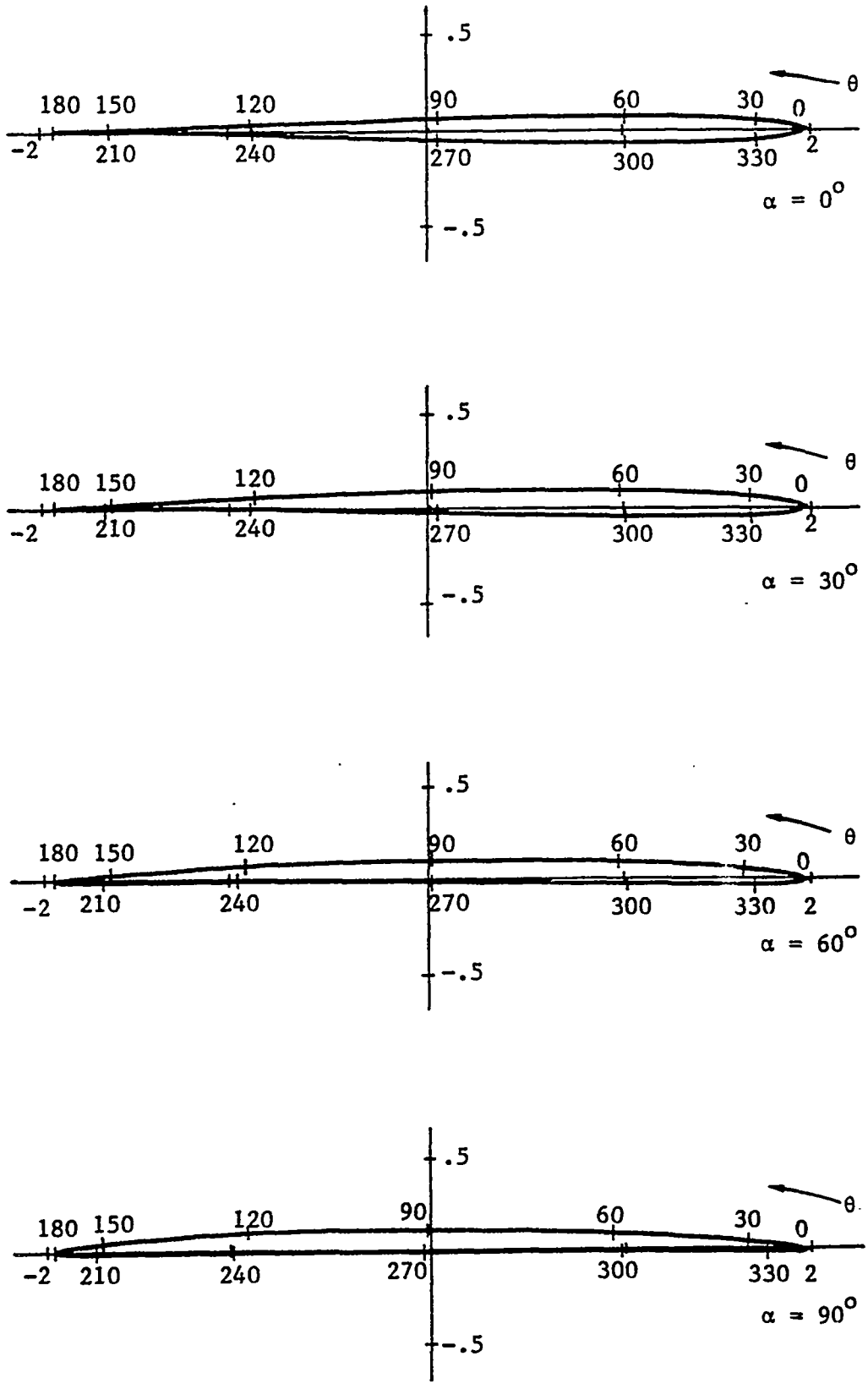

Figure 7a. Shapes of normalized airfoils defined by $\ell/a = .97$, $w_o/a = .03$ and the parameter α.

Table 5

Normalized Airfoils as a Function of the Parameter θ

$\ell/a = .97$, $w_o/a = .03$

	$\alpha = 0^o$		$\alpha = 30^o$		$\alpha = 60^o$		$\alpha = 90^o$	
θ	$\lvert z/a \rvert$	Ang(z)	$\lvert z/a \rvert$	Ang(z)	$\lvert z/a \rvert$	Ang(z)	$\lvert z/a \rvert$	Ang(z)
0^o	1.94	360.00^o	1.94	0.05^o	1.94	0.07^o	1.94	0.05^o
10^o	1.92	0.58^o	1.91	0.62^o	1.90	0.57^o	1.90	0.43^o
20^o	1.83	1.18^o	1.82	1.26^o	1.81	1.18^o	1.81	0.93^o
30^o	1.70	1.79^o	1.68	1.98^o	1.67	1.92^o	1.66	1.60^o
40^o	1.51	2.46^o	1.50	2.83^o	1.48	2.86^o	1.46	2.50^o
50^o	1.28	3.24^o	1.27	3.89^o	1.24	4.10^o	1.22	3.78^o
60^o	1.02	4.27^o	1.00	5.37^o	0.98	5.93^o	0.95	5.75^o
70^o	0.72	5.92^o	0.71	7.87^o	0.68	9.15^o	0.66	9.38^o
80^o	0.40	9.89^o	0.39	14.00^o	0.37	17.33^o	0.35	19.18^o
90^o	0.08	45.85^o	0.10	60.72^o	0.11	75.41^o	0.12	90.00^o
100^o	0.28	170.02^o	0.29	164.47^o	0.32	161.24^o	0.35	160.82^o
110^o	0.61	176.46^o	0.61	173.78^o	0.63	171.64^o	0.66	170.62^o
120^o	0.93	178.34^o	0.92	176.71^o	0.93	175.20^o	0.95	174.25^o
130^o	1.21	179.19^o	1.20	178.14^o	1.21	177.04^o	1.22	176.22^o
140^o	1.46	179.63^o	1.45	178.95^o	1.45	178.16^o	1.46	177.50^o
150^o	1.66	179.85^o	1.65	179.45^o	1.65	178.91^o	1.66	178.40^o
160^o	1.82	179.96^o	1.81	179.75^o	1.80	179.41^o	1.81	179.07^o
170^o	1.91	179.99^o	1.90	179.92^o	1.90	179.76^o	1.90	179.57^o
180^o	1.94	180.00^o	1.94	180.00^o	1.94	179.98^o	1.94	179.95^o
190^o	1.91	180.01^o	1.91	180.02^o	1.92	180.10^o	1.92	180.21^o
200^o	1.82	180.04^o	1.83	180.01^o	1.84	180.14^o	1.84	180.39^o
210^o	1.66	180.15^o	1.68	180.00^o	1.69	180.14^o	1.71	180.49^o
220^o	1.46	180.37^o	1.48	180.02^o	1.50	180.09^o	1.52	180.52^o
230^o	1.21	180.81^o	1.23	180.13^o	1.25	180.03^o	1.28	180.49^o
240^o	0.93	181.66^o	0.94	180.44^o	0.97	180.00^o	1.00	180.41^o
250^o	0.61	183.54^o	0.63	181.24^o	0.65	180.08^o	0.68	180.29^o
260^o	0.28	189.98^o	0.29	184.23^o	0.32	180.66^o	0.35	180.15^o
270^o	0.08	314.15^o	0.06	329.25^o	0.03	344.56^o	0.00	270.00^o
280^o	0.40	350.11^o	0.39	354.30^o	0.37	357.84^o	0.35	359.85^o
290^o	0.72	354.08^o	0.72	356.31^o	0.71	358.35^o	0.68	359.71^o
300^o	1.02	355.73^o	1.02	357.14^o	1.01	358.53^o	1.00	359.59^o
310^o	1.28	356.76^o	1.29	357.68^o	1.29	358.68^o	1.28	359.51^o
320^o	1.51	357.54^o	1.52	358.14^o	1.52	358.84^o	1.52	359.48^o
330^o	1.70	358.21^o	1.71	358.58^o	1.71	359.05^o	1.71	359.51^o
340^o	1.83	358.82^o	1.84	359.03^o	1.84	359.32^o	1.84	359.61^o
350^o	1.92	359.42^o	1.92	359.52^o	1.92	359.65^o	1.92	359.79^o
360^o	1.94	360.00^o	1.94	0.05^o	1.94	0.07^o	1.94	0.05^o

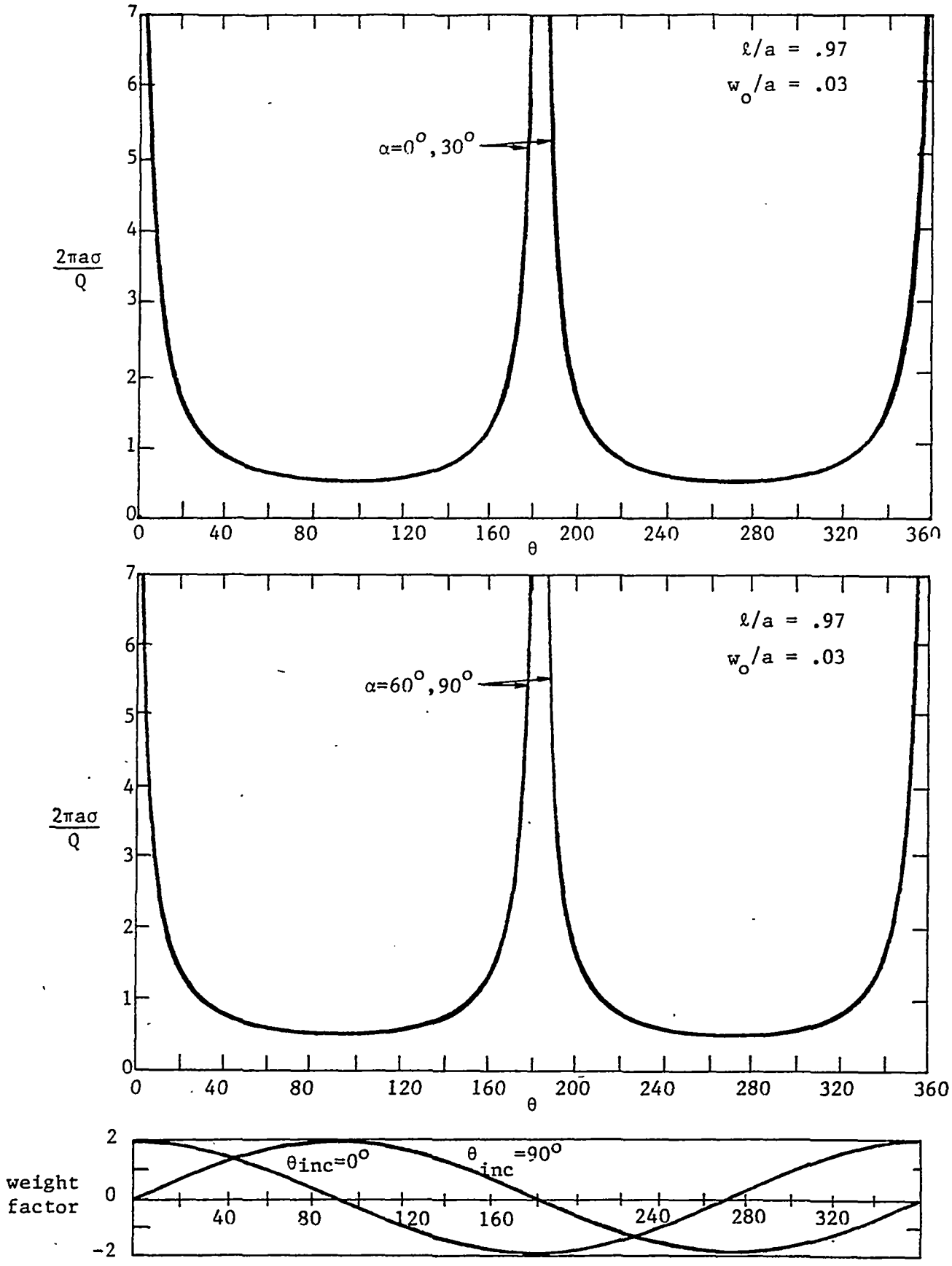

Figure 7b. The charge density on the airfoils of Figure 7a having a net charge Q per unit length, shown as a function of position. Weight functions for determining the induced surface charge due to an electric field incident on the airfoil at an angle θ_{inc} are also given.

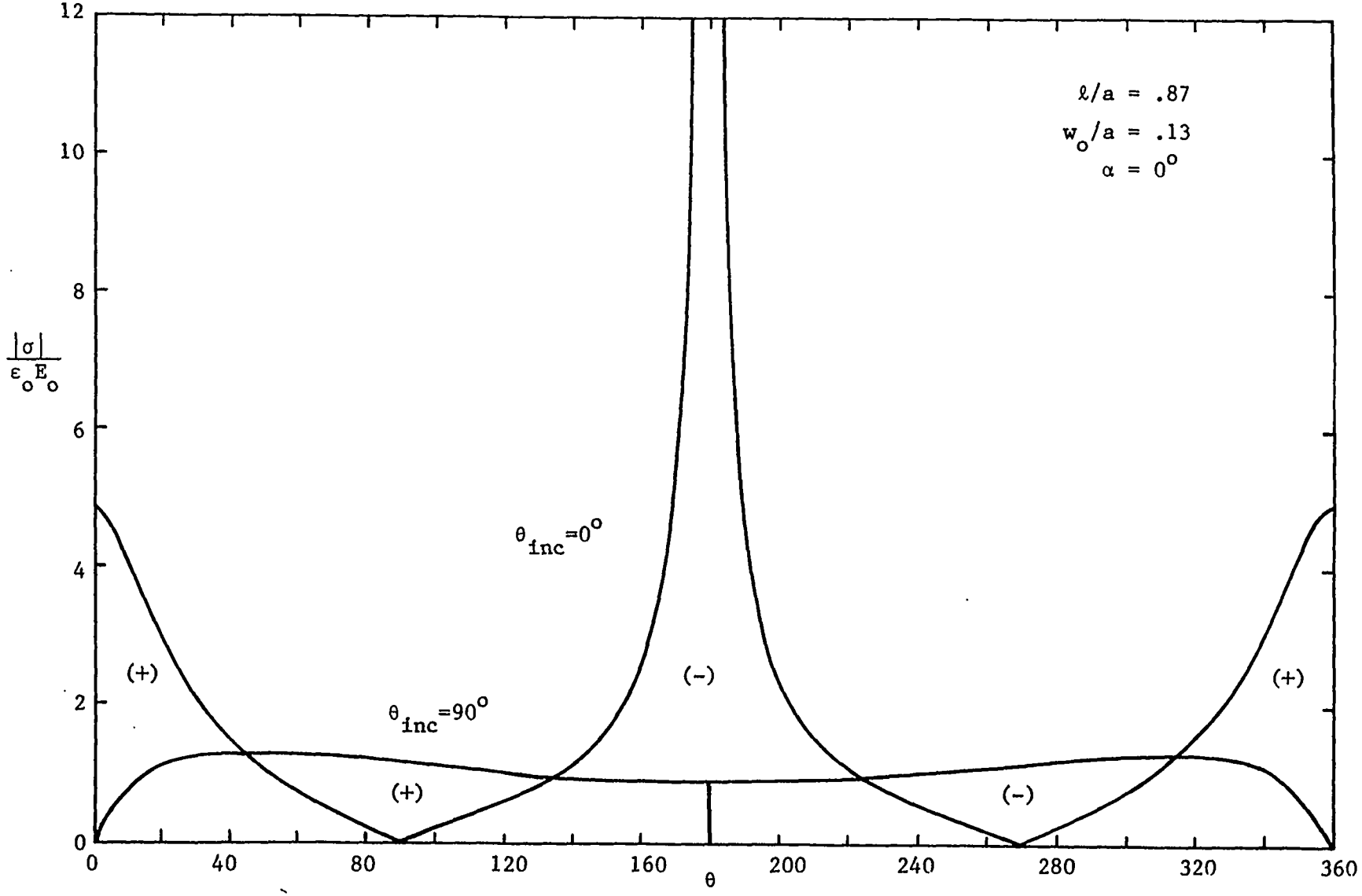

Figure 8. Charge density on the airfoil for $\alpha = 0^o$ in Figure 5a for the case of an electric field incident at $\theta_{inc} = 0^o$ and 90^o. These curves are obtained by multiplying the appropriate curve in Figure 5b by the weight factors.

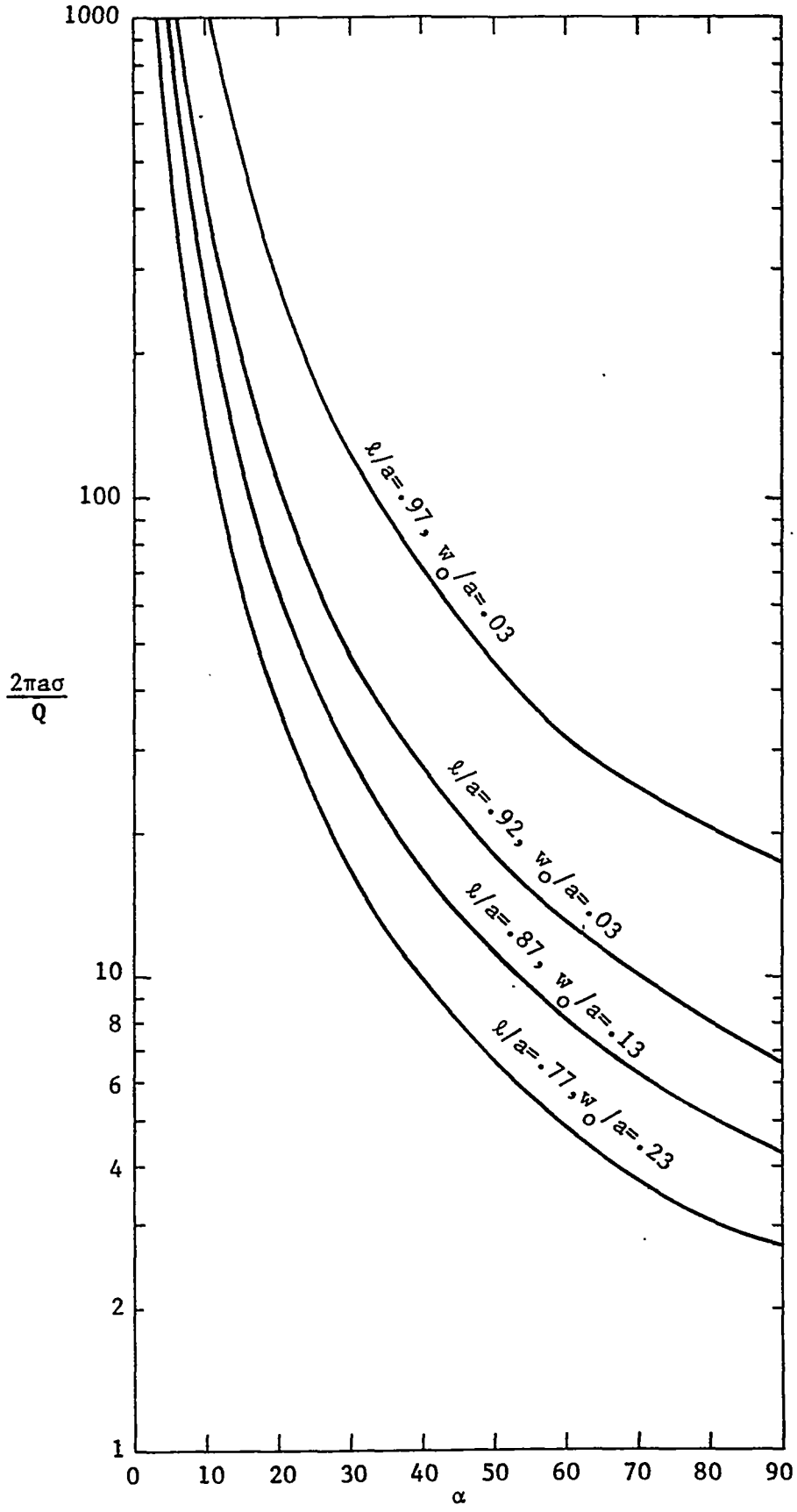

Figure 9a. Normalized charge density on the trailing edge of various airfoils having a net charge, shown as a function of the parameter α. Note the logarithimic scale.

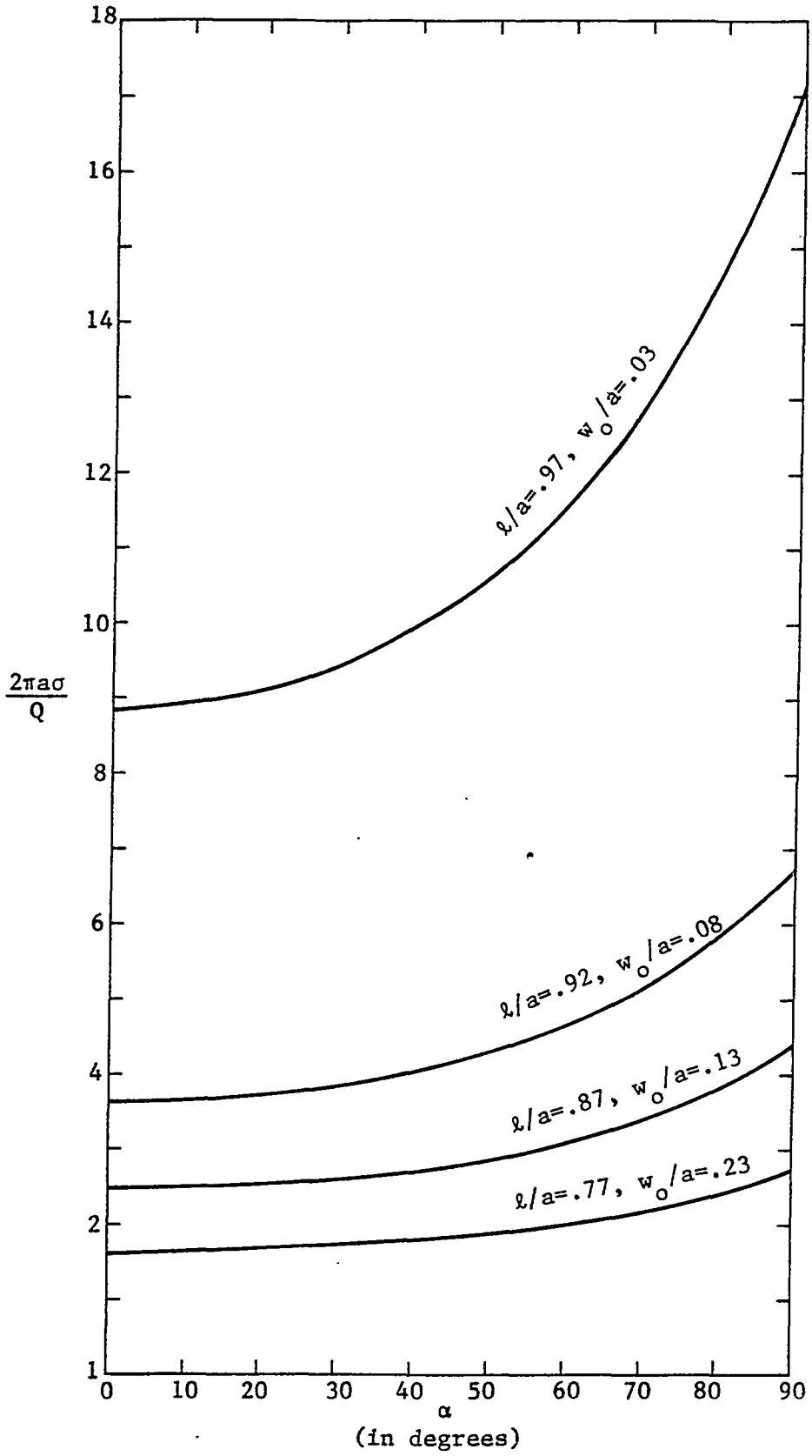

Figure 9b. Normalized charge density on the leading edge of various airfoils having a net charge, shown as a function of the parameter α.

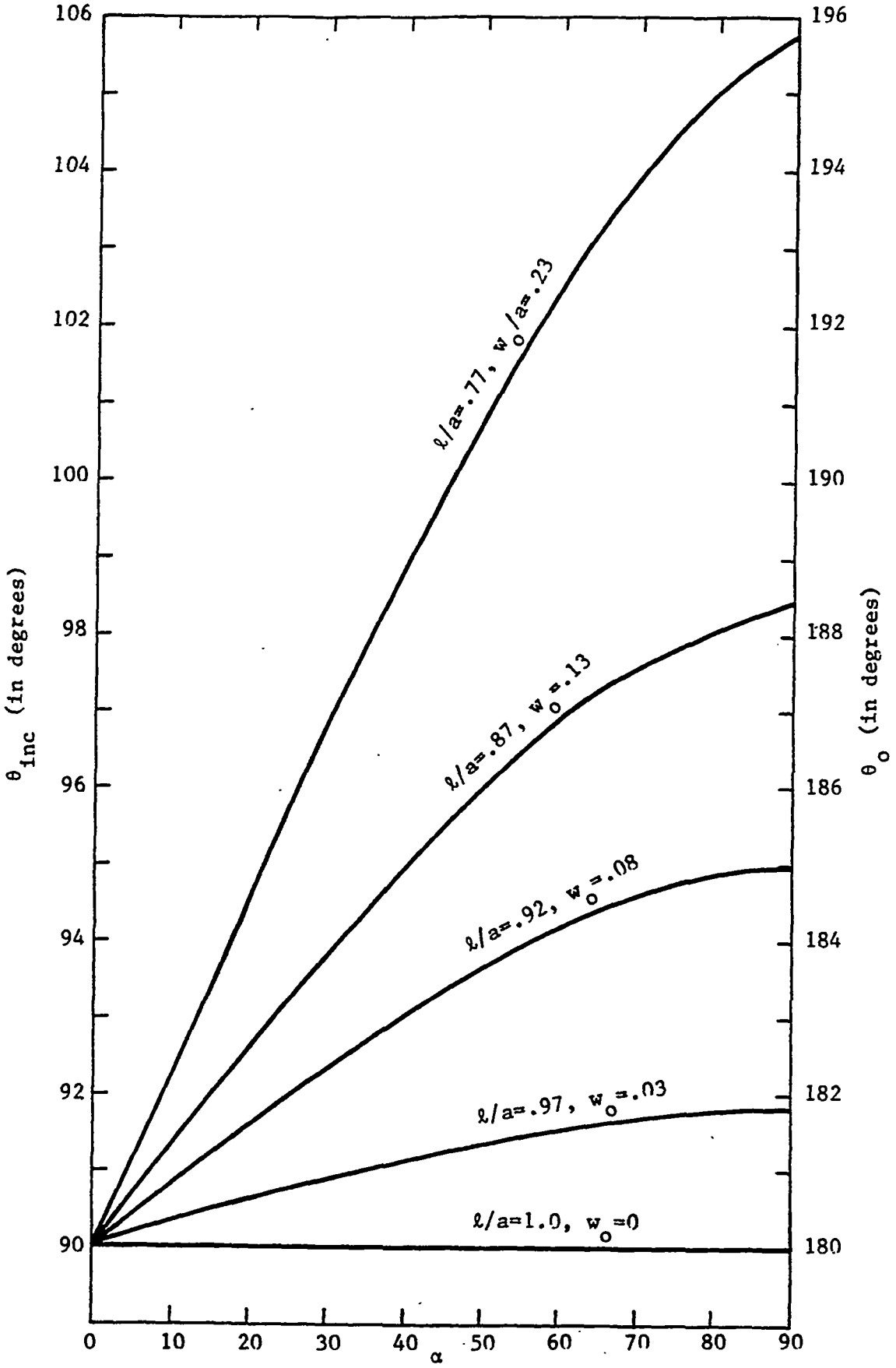

Figure 10a. Plots of θ_{inc} vs. α for a null in the induced charge at the trailing edge of various airfoils immersed in a static electric field. The value θ_o defines the location of the trailing edge of the airfoil.

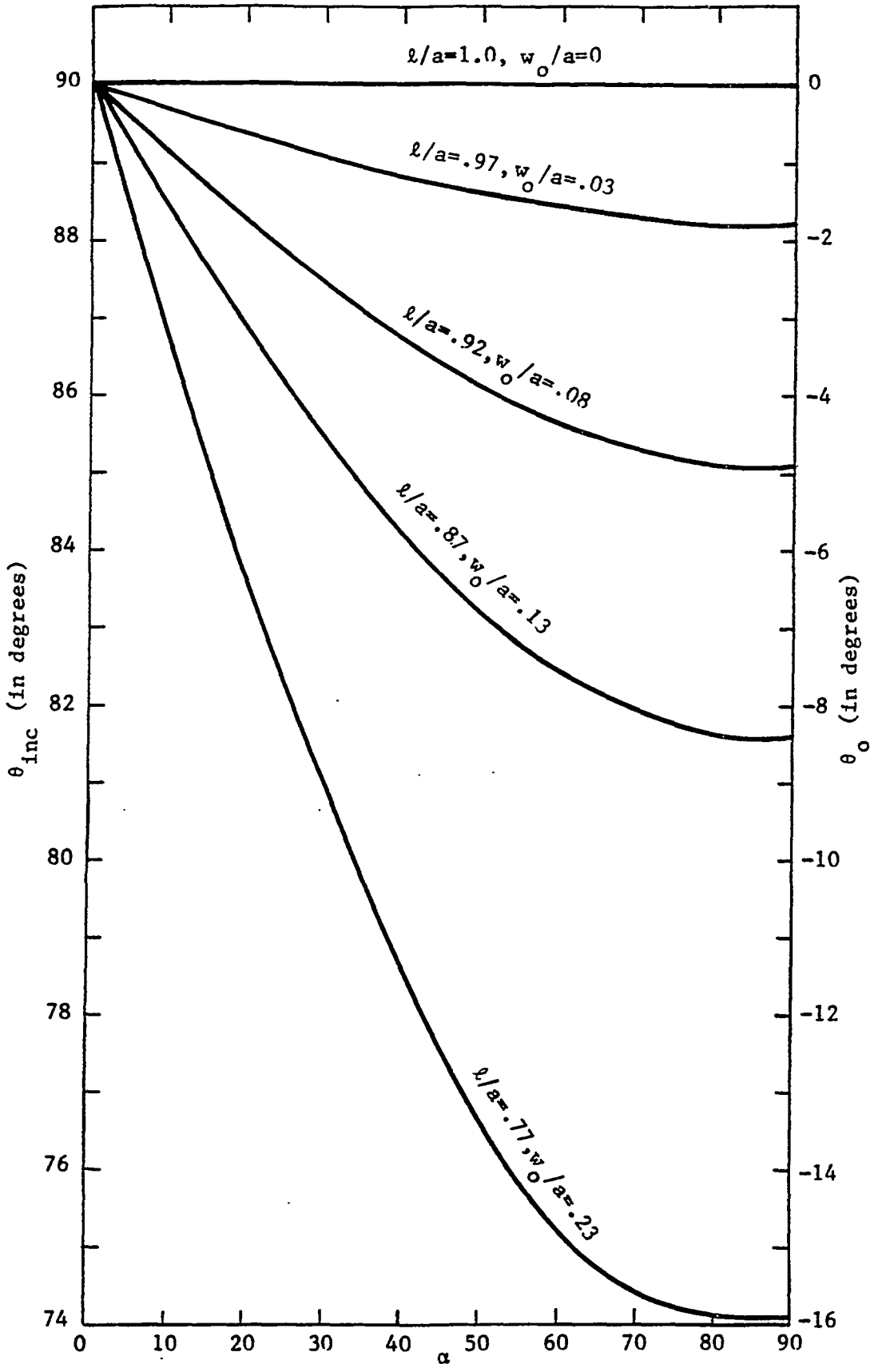

Figure 10b. Plots of θ_{inc} vs. α for a null in the induced charge at the leading edge of various airfoils immersed in a static electric field. The value θ_o defines the location of the leading edge of the airfoil.

References

1. Churchill, R. V., Introduction to Complex Variables and Applications, McGraw-Hill, New York, 1948.
2. Milne-Thompson, L. M., Theoretical Hydridynamics, MacMillan, New York, 1968.
3. Smythe, W. R., Static and Dynamic Electricity, McGraw-Hill, 2nd Ed., New York, 1950.